Mon. Not. R. Astron. Soc. **000**, 000–000 (0000) Printed 5 February 2008 (MN LATEX style file v1.4)

OH maser disc and outflow in the Orion-BN/KL region

R. J. Cohen⋆[1], N. Gasiprong,[1,2] J. Meaburn[1,3] and M. F. Graham[1].
[1] *University of Manchester, Jodrell Bank Observatory, Macclesfield, Cheshire, SK11 9DL*
[2] *Department of Physics, University of Ubon Ratchithani, Ubon Ratchithani, Thailand*
[3] *Instituto de Astronomia, UNAM, Apdo, Postal 877, Ensenada, BC 22800, Mexico*

ABSTRACT

MERLIN measurements of 1.6-GHz OH masers associated with Orion-BN/KL are presented, and the data are compared with data on other masers, molecular lines, compact radio continuum sources and infrared sources in the region. OH masers are detected over an area 30 arcsec in diameter, with the majority lying along an approximately E-W structure that extends for ∼18 arcsec, encompassing the infrared sources IRc2, IRc6 and IRc7. Radial velocities range from –13 to +42 km s^{-1}. The system of OH masers shows a velocity gradient together with non-circular motions. The kinematics are modelled in terms of an expanding and rotating disc or torus. The rotation axis is found to be in the same direction as the molecular outflow. There is an inner cavity of radius ∼1300 au with no OH masers. The inner cavity, like the H_2O 'shell' masers and SiO masers, is centred on radio source I. Some of the OH masers occur in velocity-coherent strings or arcs that are longer than 5 arcsec (2250 au). One such feature, Stream A, is a linear structure at position angle ∼45°, lying between IRc2 and BN. We suggest that these masers trace shock fronts, and have appeared, like a vapour trail, 200 yr after the passage of the runaway star BN. The radio proper motions of BN, source I and source n project back to a region near the base of Stream A that is largely devoid of OH masers. The 1612-MHz masers are kinematically distinct from the other OH masers. They are also more widely distributed and appear to be associated with the outflow as traced by H_2O masers and by the 2.12-μm emission from shocked H_2. The magnetic field traced by the OH masers ranges from 1.8 to 16.3 mG, with a possible reversal. No OH masers were found associated with even the most prominent proplyds within 10 arcsec of θ^1 Ori C.

Key words: masers – polarization – magnetic fields – stars: formation – ISM: jets and outflows – ISM:individual: Orion-BN/KL

1 INTRODUCTION

The Orion A molecular cloud (L1641) is the nearest giant molecular cloud (GMC) containing the nearest regions of massive star-formation. Because of its proximity it suffers little galactic extinction, and has been studied in far greater detail than other comparable regions in the Galaxy. The most recent formation of high–mass stars in the Orion GMC is within the Becklin–Neugebauer–Kleinmann–Low (BN/KL) region, about 1 arcmin Northwest from the Trapezium star θ^1 Ori C. The explosive nature of this event is demonstrated dramatically by the infrared H_2 and [FeII] images of Allen & Burton (1993) and more recently Kaifu et al. (2000). 'Bullets' of matter are being ejected at hundreds of km s^{-1} to form a bipolar cone of molecular 'fingers' whose axis is perpendicular to the hot core traced by NH_3 emission (Wilson et al. 2000). These 'fingers' are tipped by Herbig–Haro (HH) objects whose shocked gas is visible at optical wavelengths (see Graham, Meaburn & Redman 2003 for a recent association of these phenomena).

At radio and millimetre wavelengths there are at least two molecular outflows, one associated with the optical and near-infrared features just described, and a second low-velocity outflow first detected through proper motions of H_2O masers (Genzel et al. 1981). The powerful infrared source IRc2 was originally thought to be the source of the outflow, but more recent observations, in particular of SiO masers (e.g. Greenhill et al. 1998), suggest that radio continuum source I of Menten & Reid (1995) is the more likely outflow source. Source I is significantly offset (by ∼0.″5) to the South of IRc2.

Source I and the radio counterpart to BN have proper motions away from each other, corresponding to transverse speeds of 12 and 27 km s^{-1} respectively (Plambeck et al.

⋆ Email: rjc@jb.man.ac.uk

1995; Rodríguez et al. 2005). Here and elsewhere we assume a distance of 450 pc. The radio proper motions indicate that BN and source I were within 225 au of each other 525±30 years ago. Tan (2004) has suggested that the large proper motion of BN is due to its ejection from the θ^1 Ori C system ∼4000 years ago. Bally & Zinnecker (2005) on the other hand propose that the motions of BN and I are the result of a stellar merger ∼500 years ago, which ejected BN and produced the energy powering the molecular outflow. Further analysis of the radio proper motion data by Gómez et al. (in press) shows that a third source n also has proper motions that project back to the position on the sky where BN and source I were close, ∼500 years ago. This raises the possibility that n is the third star dynamically neccessary to eject BN from the multiple system. Distinguishing between these different possibilities is crucial to understanding the history of recent star-formation in the region.

We have observed hydroxyl (OH) masers in the Orion-BN/KL region as part of an ongoing study of masers associated with molecular outflows from massive young stars (Hutawarkorn & Cohen 2005, and references therein). OH masers have the potential to trace physical conditions, including magnetic fields which are detected and measured through Zeeman splitting and OH maser polarization. Previous MERLIN OH observations by Norris (1984) detected 80 1665-MHz masers distributed over a region of 10 arcsec, which were interpreted in terms of a rotating torus surrounding IRc2. Johnston, Migenes & Norris (1989) detected 175 masers spread over a region of 20 arcsec, with the majority in an E-W structure 14 arcsec in extent. The masers were found in clusters or 'clumps' that correlated with NH_3 emission. The present MERLIN observations more than double the number of OH masers known and show that the distribution is even more extensive in position and velocity (Section 3.1). The association of the masers with radio continuum sources is described in Sections 3.1 and 4.2, while the association with near- and mid-infrared sources is described in Section 3.3.

Secondary targets in the same MERLIN observations were the 'proplyds' (O'Dell, Wen & Hu 1993) in the vicinity of θ^1 Ori C. These are the solar system–sized circumstellar envelopes discovered by Laques & Vidal (1979) which surround low–mass YSOs (Churchwell et al 1987; Meaburn 1988; McCaughrean & Stauffer 1994; O'Dell & Wong 1996; Bally et al. 1998a). These stellar cocoons have dusty molecular disks with dense ($\geq 10^6$ cm^{-3}) surfaces ionized by the intense flux of Lyman radiation from θ^1 Ori C (see Graham et al. 2002). In these circumstances maser emission could be anticipated from the molecular disks which, if detectable, could be an important tool for investigating proto-planetary environments. Upper limits for such emission are reported in Section 3.5.

2 OBSERVATIONS

The OH observations were performed on 1998 April 27 and 28 using seven telescopes of MERLIN (the Multi Element Radio Linked Interferometer Network): the 76-m Lovell Telescope and the Mk2 telescope at Jodrell Bank, and outstation telescopes at Pickmere, Darnhall, Knockin, Defford and Cambridge. The longest baseline was 218 km, giving a minimum fringe spacing of 0.16 arcsec. Observations covered all four ground-state OH transitions, namely 1612, 1665, 1667 and 1720 MHz. A spectral bandwidth of 500 kHz was used, corresponding to a velocity range of 90 km s^{-1}. The spectral band was divided into 256 frequency channels, giving a velocity spacing of 0.35 km s^{-1}. The radial velocity at the centre of the 500-kHz band was +28 km s^{-1} with respect to the local standard of rest (lsr). Left-left and right-right circularly polarized signals from each pair of telescopes were simultaneously correlated to give LL and RR.

The OH lines were observed in pairs, 1612 and 1667 MHz for 6.5 hours on 27 April 1998 and 1665 and 1720 MHz for 8 hours on 28 April 1998. Observations consisted of 5-min scans tracking the field centre RA(B1950) $05^{\mathrm{h}}32^{\mathrm{m}}49\overset{\mathrm{s}}{.}043$, Dec. (B1950) $-05^\circ 25' 16\overset{''}{.}003$ at each OH line frequency interleaved with 4-min scans on the nearby unresolved phase calibrator source IC0539-057. Because of the faintness of the phase calibrator source it was necessary to observe it in 16-MHz bandwidth. Short ∼ 30-min scans of the point source amplitude and bandpass calibrator 2134+004 were also made. 2134+004 was also used to provide the flux scale (based on comparisons with 3C286).

The data processing and analysis procedures were carried out in B1950 coordinates, as described by Gasiprong, Cohen and Hutawarakorn (2002). Data were first edited, calibrated and corrected for gain-elevation effects using the Jodrell Bank d-programmes, and then passed into the AIPS software package. Within the AIPS package the data were further calibrated for all remaining instrumental and atmospheric effects including the instrumental polarization. Self-calibration imaging of a bright pointlike reference channel was employed to derive the final gain solutions for the 1665-MHz data. These gain solutions were then applied to the other channels. The 1612- and 1667-MHz data sets had poorer signal-to-noise and could not be self-calibrated, while at 1720 MHz no emission was detected at all. Finally, maps in each circular polarization (RHC and LHC) were produced using CLEAN algorithms in AIPS, with a restoring beam of 150 mas × 150 mas. For each data cube the pixel size was 45×45 mas^2 and the total area mapped was 1024×1024 pixels^2 (46×46 arcsec^2), centred on the position of IRc2. A second field of 512×512 pixels (23×23 arcsec^2) centred on the position of θ^1 Ori C was also searched for possible emission associated with the proplyds.

The rms-noise in the final maps was 30-50 mJy beam^{-1}, so only masers brighter than ∼0.1 Jy could be detected. The masers were all unresolved at 150-mas resolution. Positions of maser features were determined by fitting two-dimensional Gaussian components to the brightest peaks in each channel map and taking flux-weighted means across the channels showing emission from each particular feature. Final B1950 coordinates of masers were then converted to J2000 using the software package coco. The errors in the relative positions are typically 10 mas, while the absolute positions have a possible systematic error of 20 mas due to phase-transfer from the reference source.

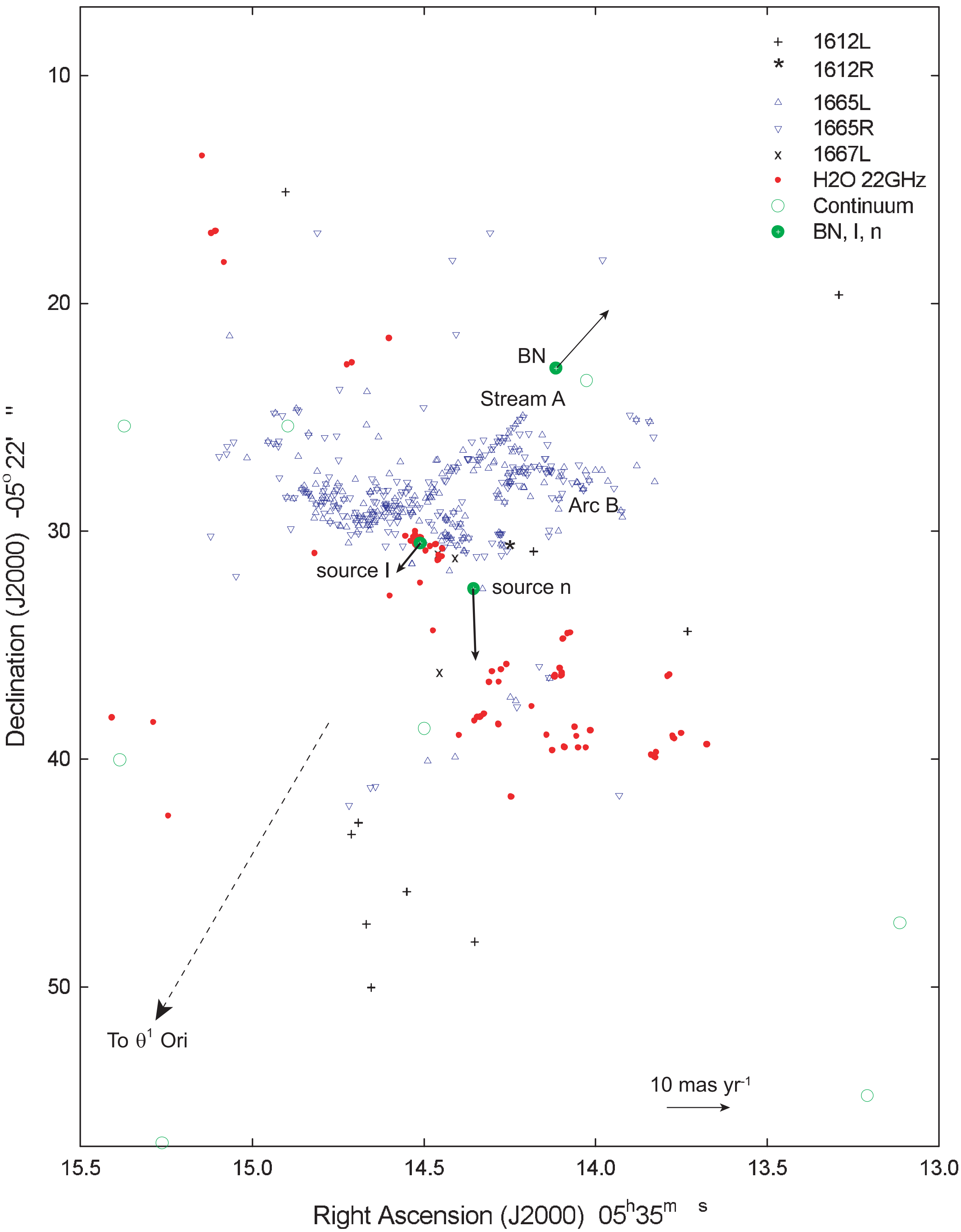

Figure 1. Positions of OH masers (blue symbols, this paper), H_2O masers (red symbols, Gaume et al. 1998), and compact continuum sources (green circles, Zapata et al. 2004) in Orion-BN/KL. The central region around IRc2 and radio source I is shown on an expanded scale in Fig. 2. The radio continuum sources BN, I and n are highlighted as filled green circles, and their proper motions are indicated schematically (data from Rodríguez et al. 2005 and Gómez et al. 2005). The direction to θ^1 Ori C is indicated by the dashed arrow.

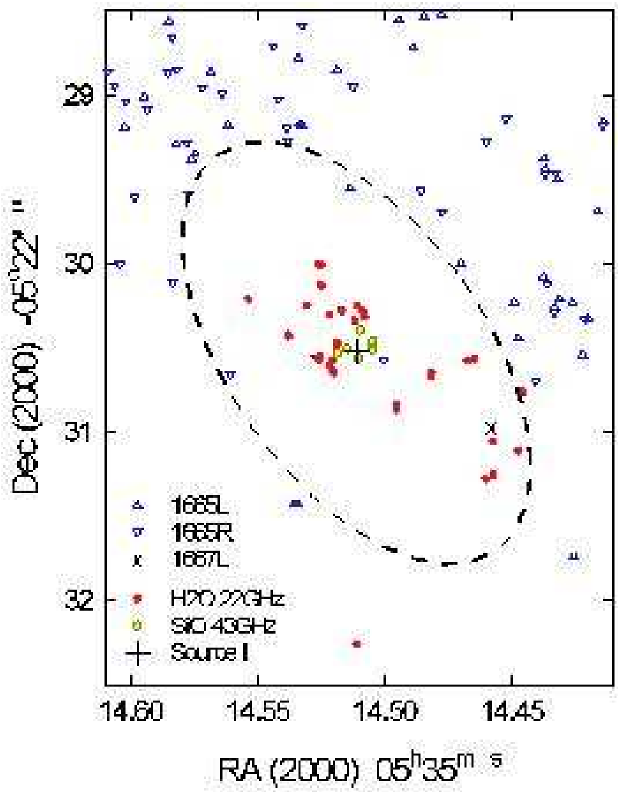

Figure 2. Positions of OH masers (blue symbols, this paper), H_2O masers (red symbols, Gaume et al. 1998) and SiO maser clusters (yellow symbols, Doleman et al. 1999) in the central region of Orion-KL, near radio source I (Menten & Reid (1995). The position for source I corresponds to epoch 2000 (Rodríguez et al. 2000). The dashed ellipse corresponds to a ring with rotation axis at position angle –35°and inclination angle 58°to the line-of-sight, centred on radio source I (see Section 4.1).

3 RESULTS

3.1 Maser distribution in Orion-BN/KL

We detected 11 masers at 1612 MHz, 430 masers at 1665 MHz, 3 masers at 1667 MHz (LHC only) and no masers at 1720 MHz. The positions and velocities are given in Table 1. To facilitate comparison with other data, we give both the B1950 coordinates and the J2000 coordinates. The maser distribution is shown in Fig. 1 in J2000 coordinates. The OH masers are spread over a region 30 arcsec in extent, corresponding to ∼13500 au. The radial velocities range from –13 to +42 km s^{-1}. The distribution is more extensive in both angular scale and velocity range than found in previous work. However most of the emission comes from the dominant E-W structure noted by Norris (1984) and Johnston et al. (1989).

One striking aspect of the new maps is that many of the OH masers lie in semi-continuous streams or arcs, of which the most prominent are labelled Stream A and Arc B in Fig. 1. Stream A stretches from RA (2000) $05^h35^m14\overset{s}{.}2$, Dec. (2000) $-05°22'25''$to $05^h35^m14\overset{s}{.}5$, $-05°22'28''$, and includes the maser 'clump' NW1 identified by Johnston et al. (1989). The radial velocities are approximately constant, around +21±2 km s^{-1}. Arc B stretches from $05^h35^m14\overset{s}{.}1$, $-05°22'28''$to $05^h35^m14\overset{s}{.}3$, $-05°22'28''$, and includes the maser clumps NW2 and NW3 of Johnston et al. (1989). The radial velocities cover a wide range, from ∼-7 km s^{-1} in the East to ∼+10 km s^{-1} in the West. These streams or arcs are large-scale features, with angular sizes of ∼5 arcsec that correspond to ∼2250 au. We argue that they trace large-scale shocks or ionization fronts (Section 4.2).

The distribution of H_2O masers from Gaume et al. (1998) is also shown in Fig. 1. The OH and H_2O masers have complementary distributions, with almost no overlap. An expanded plot of the crowded central region is shown in Fig. 2, revealing the same situation on the small scale. The H_2O masers in this region are the so-called 'shell' masers that were not detected in the VLBI measurements by Genzel et al. (1981). There is an elliptical zone of avoidance centred on source I, within which there are very few OH masers, but the H_2O 'shell' masers and SiO masers are found. The H_2O 'shell' masers lie inside the dashed ellipse in the figure, while nearly all of the OH masers lies outside the ellipse. The position angle and inclination angle of the ellipse were chosen to match the model fitted to the OH masers in Section 4.1.

Fig. 2 also shows the positions of the SiO maser clusters mapped by Doeleman, Lonsdale & Pelkey (1999). The SiO masers cluster tightly around the position of the radio source I (Menten & Reid 1995), with the H_2O 'shell' masers surrounding them. The relative location of SiO, H_2O shell and OH masers at increasing distances from the central source I is similar to that found for these masers in the circumstellar envelopes of post-AGB stars, which has a natural explanation in terms of excitation by a powerful central source (Chapman & Cohen 1986).

The positions of compact radio continuum sources in the region are plotted in Fig. 1 as open green circles (data from Zapata et al. 2004), with sources I, n and BN highlighted as filled green circles. Apart from source I, which is at the centre of the SiO and H_2O 'shell' maser distributions and the OH zone of avoidance, there is another association of OH masers with a compact radio continuum source that is noteworthy, namely a striking association between Stream A and BN. The stream points directly towards BN (away from IRc2), in the direction of BN's proper motion (shown schematically by the arrow in Fig. 1). This is discussed further in Section. 4.2. Finally we note a possible weaker association of source D of Menten & Reid (1995) (source 21 of Zapata et al.), near RA (J2000) = $05^h35^m14\overset{s}{.}90$, Dec. (J2000) = $-05°22'25\overset{''}{.}4$, with a cluster of OH masers, corresponding to 'clump NE1' of Johnston et al. (1989). The radial velocities are centred near +8 km s^{-1}.

Further study of Fig. 1 reveals that the OH 1612-MHz masers are distributed differently from the mainline 1665- and 1667-MHz masers. Most of the OH 1612-MHz masers are found a long way from the centre, in the outskirts of the OH maser region, and they are spatially separated from the other OH masers. Their far-flung distribution is strikingly different from that of the other OH masers, but similar to that of the H_2O masers. This similarity is reinforced by kinematic similarities.

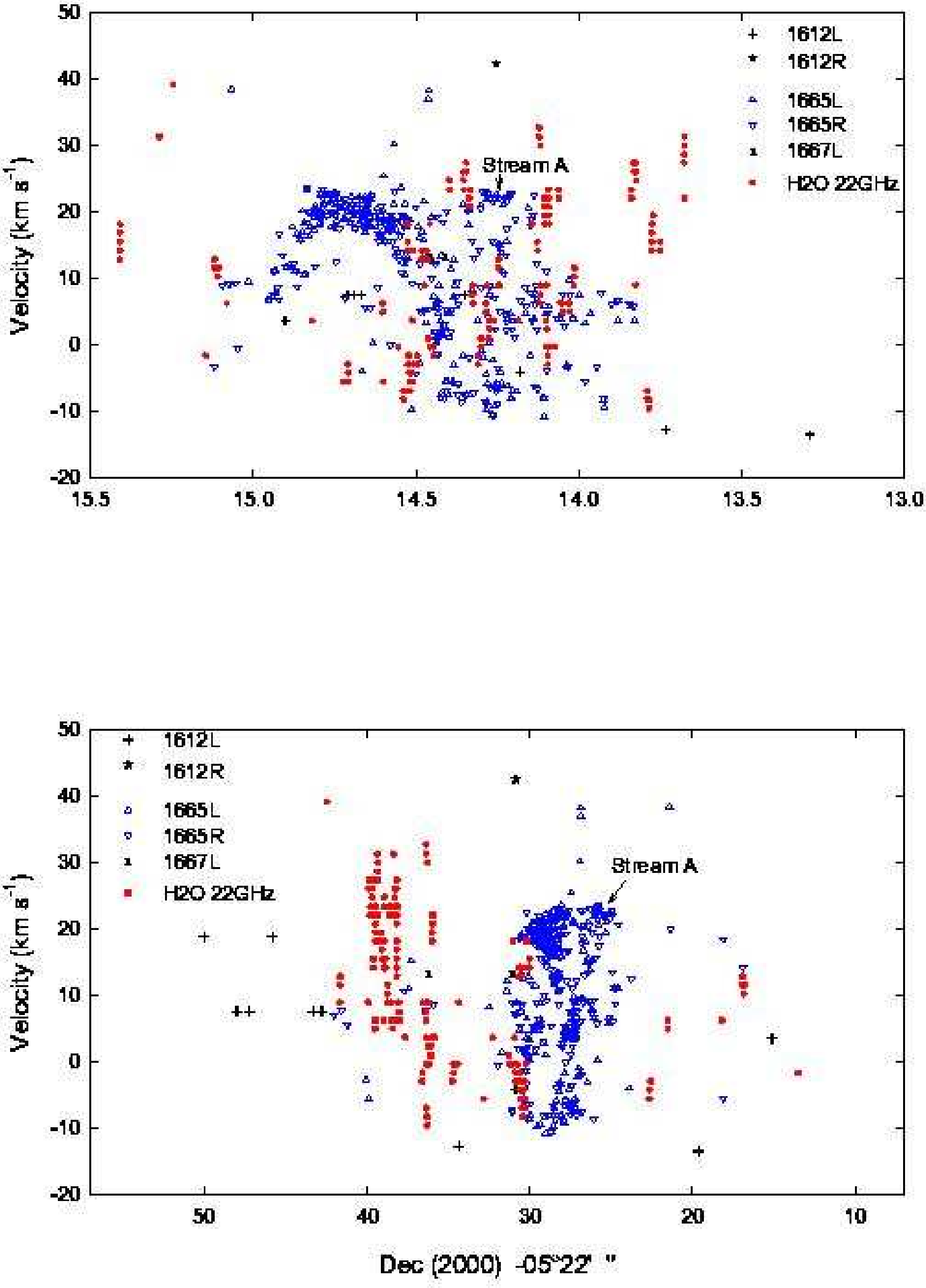

Figure 4. Position-velocity plot showing declination (J2000) and radial velocity for the OH masers (blue symbols, this paper) and the H_2O masers (red symbols, Gaume et al. 1998) in Orion-BN/KL.

3.2 Maser kinematics

The complex kinematics of the Orion-BN/KL masers are summarized in the position-velocity diagrams Figs. 3 and 4. Fig. 3 shows RA vs. $V_{\rm lsr}$ for the OH and H_2O masers. There is a clear contrast between the two species: the OH masers show a dominant rotational pattern, in which the radial velocities drop from +20 km s^{-1} in the East to 0 km s^{-1} in the West, while the H_2O masers show a dominant expansion pattern, with highly red-shifted or blue-shifted masers equally likely to occur to the East or West. This is consistent with the well known expansional proper motions of these masers (Genzel et al. 1981; Gaume et al. 1998). The OH rotational pattern is clearest at right ascensions greater than $05^{\rm h}35^{\rm m}14\overset{\rm s}{.}5$, and more disturbed at right ascensions less than this. Stream A has a velocity greatly different from the rotational pattern, as indicated in Fig. 3. We note that the radial velocity of Stream A, +21 km s^{-1}, is the same as that of BN and its circumstellar nebulae within 25 au (Scoville et al. 1983).

Fig. 4 shows a Dec-$V_{\rm lsr}$ plot. The OH masers trace a dominant inclined elliptical pattern, centred on Dec. (2000) $-05^\circ22'29''$and $V_{\rm lsr}$ = +6 km s^{-1}. Radial velocities rise abruptly from 0–10 km s^{-1} in the South to +20 km s^{-1} to the North of Dec. (2000) $-05^\circ22'29''$. The 'hole' in the centre of the Dec-$V_{\rm lsr}$ ellipse suggests that in addition to rotation there is an expansional component of motion of similar magnitude. The locations of OH and H_2O masers in this diagram are again complementary.

The OH 1612-MHz masers are kinematically and spatially distinct from the 1665- and 1667-MHz masers. This is particularly clear in Fig. 4, where they are well separated in both declination and velocity, appearing at the extremes of both coordinates, well separated from the rotating and expanding ring signature of the mainline masers. The kinematic pattern is similar to but even more extensive than that of the H_2O masers, suggesting that outflow rather than rotation is the dominant motion.

The OH distribution and kinematics are modelled in Section 4.1.

3.3 Comparison with Infrared Data

The distribution and kinematics of the dominant OH emission show a degree of symmetry about the position of IRc2 and radio source I, and a radial velocity of ∼8 km s^{-1}, as noted by previous authors cited in the introduction. The OH masers encompass IRc2, 3, 6 and 7. The availability of high resolution infrared data allows us to examine in more detail the correspondences of the OH masers with the powerful mid-infrared sources and with near-infrared bullets in the molecular outflow.

3.3.1 Comparison with 12.5-μm Keck and 11.7-μm Gemini Data

Shuping, Morris & Bally (2004) have published a high resolution ($0\overset{''}{.}38$) mid-infrared image of the Orion BN/KL region obtained with the Keck I telescope at 12.5-μm. Fig. 5 is a composite plot showing the OH masers (this paper) superimposed on Fig. 5 of Shuping et al. (2004). This shows several surprising results. Firstly, OH masers cluster around IRc2, but they avoid the actual source position (relative coordinates (+5″, –7″) in this diagram), which lies in the zone of avoidance noted in Section 3.1. Secondly, Stream A points directly away from IRc2 towards the dominant mid-infrared source BN (at the origin), at position angle ∼45°. Stream A runs through a region devoid of mid-infrared emission. The direction from IRc2 to BN is parallel to the proper motions recently measured for BN and radio source I by Rodríguez et al. (2005). It is also the projected direction of the large-scale molecular outflow. Thirdly, Arc B curves parabolically around the extended source IRc6 (near (+1″,–4″) in this figure), in a manner that suggests a close physical association. This confirms and extends the result of Johnston et al. (1989).

Smith et al. (2005) have published a high-resolution 11.7-μm mosaic image of the inner Orion nebula obtained with the Gemini South telescope. The only close correlation (better than 2 arcsec) of any of the OH 1.6-GHz masers listed in Table 1 with the 11.7-μm point sources listed by Smith et al. (2005) is the 1612L maser number 10, at RA (J2000) = $05^{\rm h}35^{\rm m}14\overset{\rm s}{.}6533$, Dec. (J2000) = $-05^\circ22'50\overset{''}{.}022$, which has a radial velocity of +18.9 km s^{-1}. The corresponding IR source is at $05^{\rm h}35^{\rm m}14\overset{\rm s}{.}67$, $-05^\circ22'49\overset{''}{.}5$. Smith et al. (2005) describe the latter as 'an embedded IR source with no optical ID'. None of the 27 known proplyds that correlate with 11.7-μm point sources in Smith et al. (2005) are identified here as maser sources.

3.3.2 Comparison with 2.12-μm Subaru Data

The locations of the OH masers relative to the well-studied molecular outflow are shown in Fig. 6. The infrared H_2 2.12-μm images presented here were taken with the Subaru Telescope as part of its astronomical first light programme (Kaifu et al. 2000). The data were taken on 1999 January 11, 13 and March 6 using the Cooled Infrared Spectrograph and Camera for the OH-suppression spectrograph, CISCO (Motohara et al. 1998).

The 2.12-μm image shown in Fig. 6 is a 150″× 150″section of the original $5' \times 5'$ mosaic (provided by Masa Hayashi). In order to overlay the OH maser positions onto the Subaru image, it was first necessary to astrometrically register the image with the J2000 coordinate system. This was done using > 600 stars from the catalogue of Hillenbrand & Carpenter (2000) and the Starlink GAIA software package. A computer programme was then written to read the B1950 OH maser positions and convert them to J2000 coordinates using the Starlink Astrometry Library and produce a catalogue that was readable by the GAIA software package. The positions were then overlaid using GAIA.

The 1665- and 1667-MHz masers (shown by dot and cross symbols respectively) are concentrated towards the highly obscured IRc2 region. In general they show little correspondence with features in the near-IR map. However the 1612-MHz masers (+) correspond with fingers of H_2 emission in the molecular outflow. This association is seen more clearly in Fig. 7, which shows the central region on an expanded scale. The 1612-MHz masers show a strong association with fingers of H_2 emission in the molecular outflow, particularly in the South, near RA (J2000) $05^{\rm h}35^{\rm m}14\overset{\rm s}{.}7$, Dec. (J2000) $-05^\circ22'46''$, where 6 (half) of the 1612-MHz masers are found. Three 1665R masers (numbers 63, 64 and 76 in

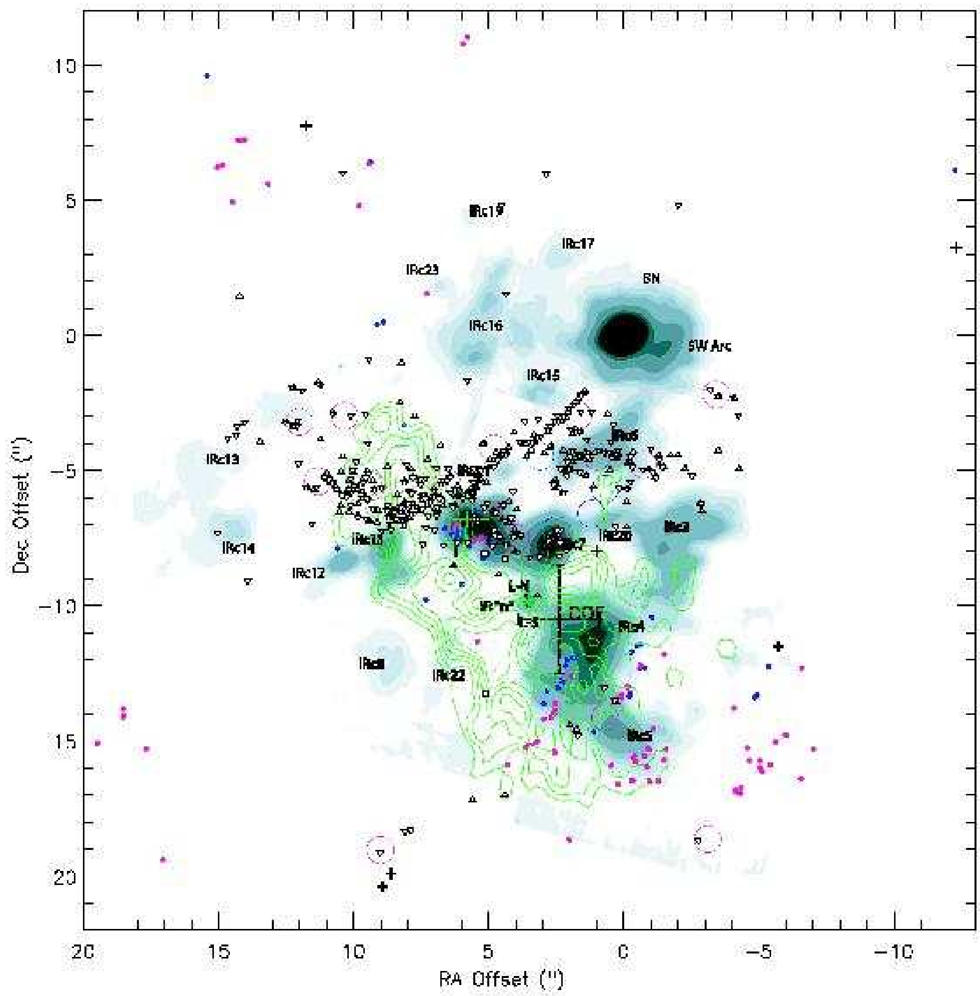

Figure 5. Positions of OH masers (black symbols as in Fig. 1) overlaid on the 12.5-μm image (greyscale) taken with the Keck Telescope by Shuping et al. (2004), adapted from their Figure 5. The open circles show the positions of OH maser clumps identified by Johnston et al. (1989). Red and blue dots indicate H_2O masers from Gaume et al. (1998) and Genzel et al. (1981), with red indicating radial velocity greater than +5 km s^{-1} and blue indicating radial velocity less than +5 km s^{-1}. The green contours show NH_3 (J,K) = (4,4) emission associated with the 'hot core', from Wilson et al. (2000). Offsets are relative to the position of the BN object: RA (J2000) = 05^{h}35^{m}14^s.117, Dec. (J2000) = –05°22′22″.9. IRc2 is near (+5″, –7″) and IRc6 is near (+1″,–4″).

Table 1) are found nearby, and may also be associated. This is the first time that clear counterparts to interstellar OH masers have been seen. It is not clear, however, why these particular H_2 emission fingers should have OH counterparts, while many others do not.

3.4 Zeeman Splitting and Magnetic Fields

The data were searched for possible Zeeman pairs of opposite circular polarization, with radial velocities differing by more than 0.8 km s^{-1} (to exclude linearly polarized features) and lying within 30 mas of each other. The results are given in Table 2. We estimate the chance of a false association to be no more than 4 percent.

The magnetic fields range from –3.5 mG (directed towards us) to +16.3 mG. In Fig. 8 we plot the magnetic field values as a function of position on the sky, together with values from previous interferometric OH Zeeman measurements (Hansen & Johnston 1983; Norris 1984; Johnston et al. 1989). The present data suggest that in addition to the overall field of 1–3 mG directed away from us, there may also be regions of higher field strength (Z_4), and that the field direction may reverse (Z_3). The field reversal is seen at only a single point, and not on the larger-scale that is found in other bipolar outflow sources (Blaskiewicz et al. 2005; Hutawarakorn & Cohen 2005, and references therein). More data are needed to confirm these findings.

3.5 Search of the Proplyd Region

A search of a 23 arcsec×23 arcsec region around θ^1 Ori C was made, but no OH masers with peak flux densities ≥0.1 Jy

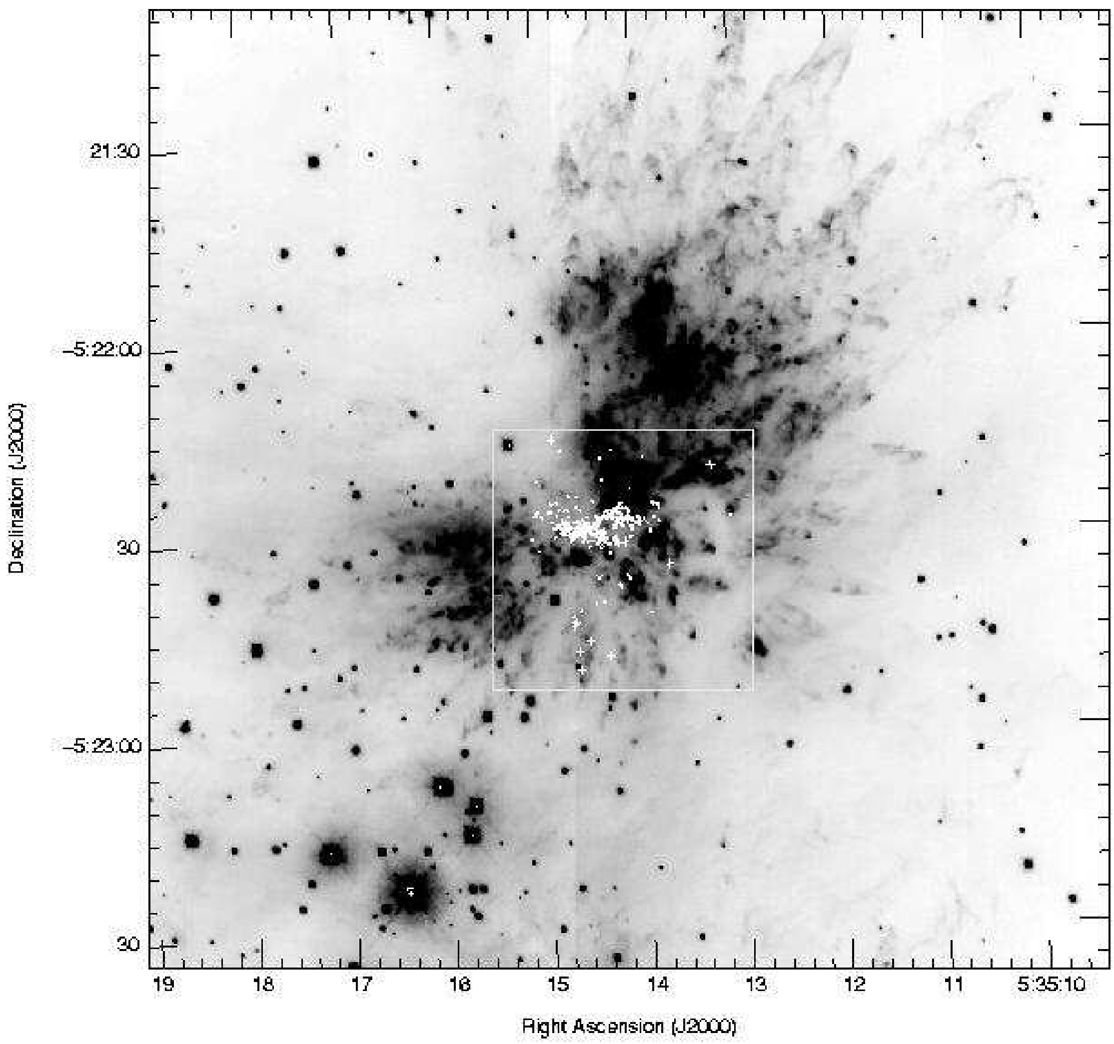

Figure 6. Positions of the OH masers in Orion-BN/KL, overlaid on the infrared 2.12-μm H_2 image taken with the Subaru Telescope by Kaifu et al. (2000), showing the relationship of the masers to the outflow (Section 3.3). The 1665-MHz masers (.) and the 1667-MHz masers (x) lie in an expanding and rotating disc or torus centred on IRc2 and source I (Section 4.1), while the 1612-MHz masers (+) have a more widespread distribution. The area in the box is shown on an expanded scale in Fig. 7.

were found, even near the most prominent proplyds (LV 1–6). The densities in these regions have been estimated to be 10^5–10^6 cm^{-3} (Section 4.4), which are typical of OH maser sources, while the temperatures are estimated to be 200–350 K (Hayward, Houck & Miles 1995), which are somewhat higher than usually encountered in OH maser sources (e.g. Cragg, Sobolev & Godfrey 2002). The non-detection of OH masers might be explained by a low OH column density, which could arise through chemical evolution (e.g. Rodgers & Charnely 2001).

4 DISCUSSION

4.1 Kinematic Model for OH 1665-MHz Masers

For our kinematic modelling we used only the 1665-MHz masers. The celestial coordinates and radial velocities of the OH masers give incomplete information on the three-dimensional source geometry and motions. The OH maser positions are essentially the x- and y-components of each maser spot, but the z-coordinate is unknown. The radial velocity of a maser is related to the unknown velocity field and the (x, y, z) coordinates of the maser. We modelled the source using a simple kinematic model which was fitted to the data using the Control Random Search technique (Price 1976). The model enables us to find the z-coordinate for

Table 2. Possible OH Zeeman pairs in Orion.

Zeeman Pair	Transition	$V_{\rm lsr}$ km s^{-1}	RA (1950) $05^{\rm h}32^{\rm m\ s}$	Dec. (1950) $-5°:24':\ ''$	RA (2000) $05^{\rm h}35^{\rm m\ s}$	Dec. (2000) $-5°:22':\ ''$	$S_{\rm pk}$ (Jy)	B mG
Z_1	1665L	21.98	46.8077	19.522	14.2830	26.065	0.18	+1.8
	1665R	23.06	46.8102	19.504	14.2855	26.047	0.10	
Z_2	1665L	18.13	47.3239	21.992	14.7984	28.572	0.10	+3.6
	1665R	20.24	47.3210	22.020	14.7954	28.600	0.38	
Z_3	1665L	15.67	46.7458	19.896	14.2210	26.434	0.14	–3.5
	1665R	13.56	46.7487	19.915	14.2239	26.454	0.22	
Z_4	1665L	11.59	46.9193	23.131	14.3934	29.682	0.26	+16.3
	1665R	1.96	46.9203	23.109	14.3944	29.660	0.10	
Z_5	1665L	0.30	46.8021	23.549	14.2761	30.092	0.58	+3.6
	1665R	2.43	46.7989	23.565	14.2729	30.108	1.48	

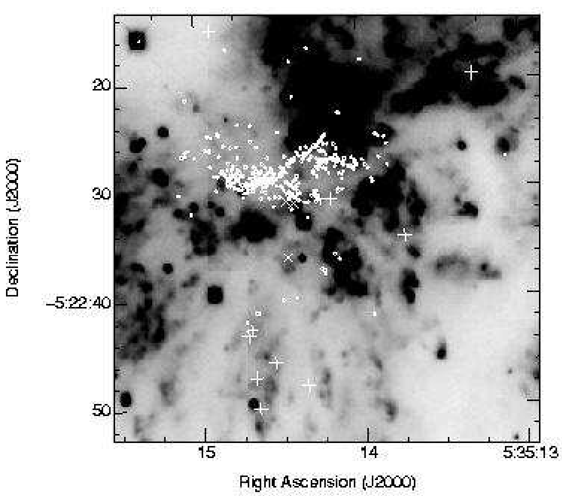

Figure 7. Expanded view of the central region of Fig. 6, showing the positions of OH masers overlaid on the infrared 2.12-μm H_2 image taken with the Subaru Telescope by Kaifu et al. (2000). The 1612-MHz masers (+) are associated with fingers of H_2 emission in the molecular outflow.

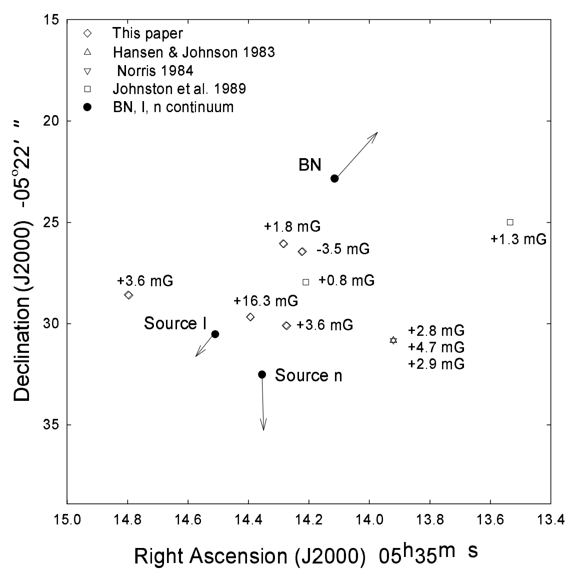

Figure 8. Magnetic field measurements in the Orion-BN/KL region from OH maser Zeeman splitting (present paper, plus references indicated in the legend). The locations and schematic proper motions of the continuum sources BN, I and n are shown for reference, as in Fig. 1.

each maser from the radial velocity and the velocity field, and so produce a three-dimensional view of the OH maser distribution (Fig. 9).

We assumed, for modelling purposes, that IRc2 is at the kinematic centre. However the results would not be affected if radio source I were taken as the centre. We estimate that the kinematic centre of the OH masers is uncertain to ~1 arcsec. The masers were assumed to have a uniform expansion velocity $V_{\rm exp}$ away from IRc2, centred on an unknown radial velocity $V_{\rm z0}$, plus solid body rotation corresponding to $V_{\rm rot}$ at 1-arcsec separation from IRc2. The rotation axis is tilted by an angle α about the y-axis and an angle β about the x-axis from the $x-z$ plane (following Reid et al. 1988). The parameters $V_{\rm exp}$, $V_{\rm z0}$, $V_{\rm rot}$, α and β were the five unknowns. For each maser and each position in the five-dimensional parameter space, we compared the observed and calculated radial velocity $V_{\rm lsr}$ and found the z-position where the absolute value of the residual was minimized (allowing the maser to lie anywhere along the z-axis, with a distance corresponding to 30 arcsec of IRc2). The five-dimensional parameter space was searched, within a reasonable domain, using a random number generator to sample the parameters. The position in five-parameter space where the sum of the (absolute) velocity residuals is minimized was thereby located. The best fitting model has the parameter values given in Table 3. The angles correspond

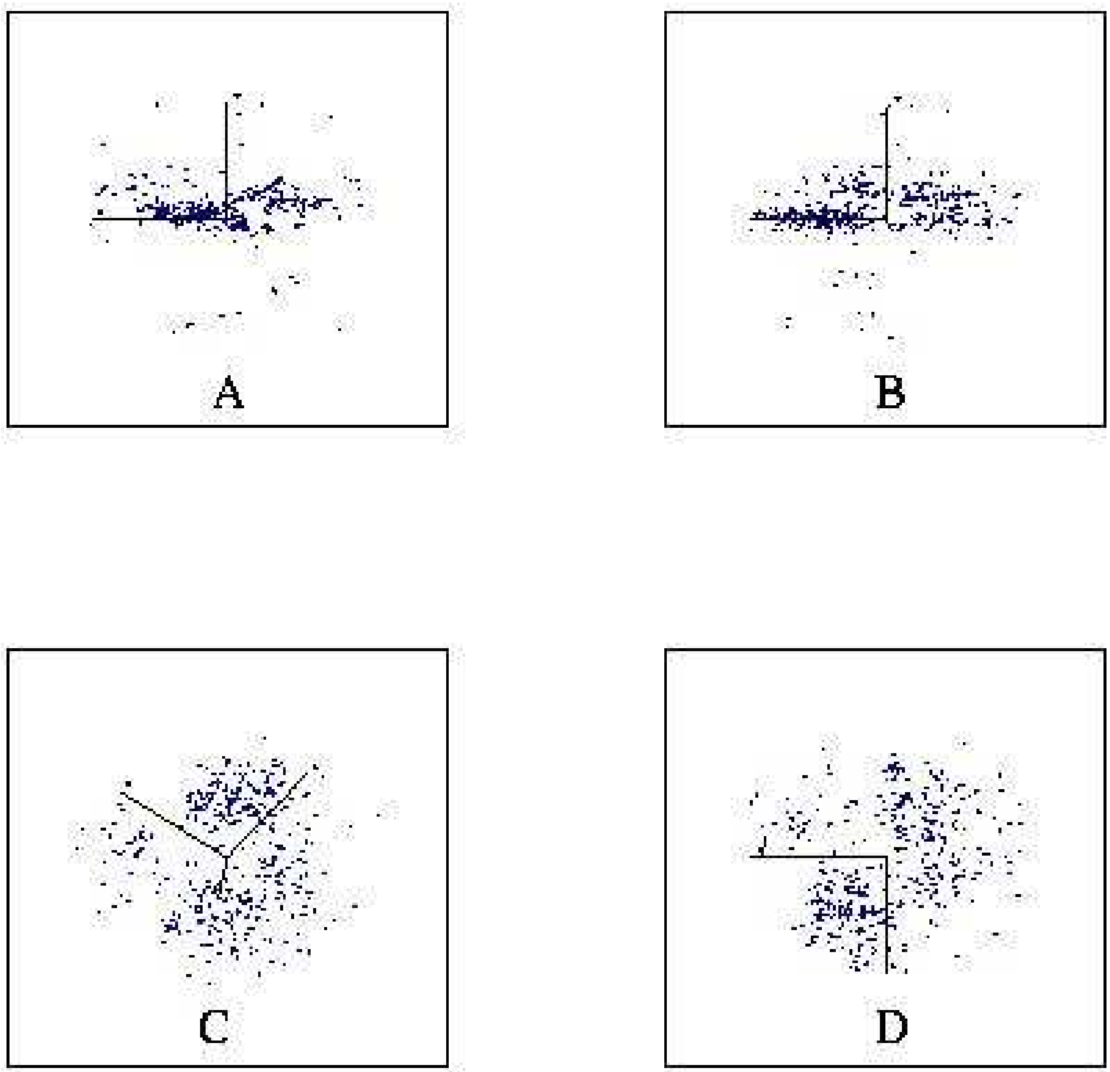

Figure 9. Three-dimensional view of the 1665-MHz OH masers in Orion-KL, according to the kinematic model that was fitted (Section 4.1). The $x-$ and $y-$axes correspond to RA and Dec, while the $z-$axis is in the line-of-sight direction. Box A shows the view in the $x-y$ (RA–Dec) plane looking in the $+z-$direction, box B shows the view looking in the $+x-$direction (increasing RA), box C shows the view looking along the rotational axis of the best-fitting model, and box D shows the view looking down the $y-$axis (decreasing Dec.).

to a rotation axis inclined at 58°to the line-of-sight with a position angle on the sky of –35°. A disc at this orientation is plotted in Fig. 2, where it fits neatly inside the 'hole' in the OH maser distribution that is centred on source I.

Using the kinematic model we constructed views of the three-dimensional distribution of OH 1665-MHz masers, which are shown in Fig. 9. The masers lie in an irregularly filled torus, at radial distances ranging from 430 au to 13200 au, with a mean radius of 6200 au. There is a well defined inner cavity, of radius $\sim$1300 au. This cavity corresponds spatially with the SiO flared disc region mapped by Wright et al. (1995, 1996), which has a radial velocity range of -10 to $+20$ km s^{-1} that is roughly consistent with the range of -12 to $+30$ km s^{-1} given by our kinematic model. The distribution in radial distance R$''$ from the rotation axis is plotted in Fig. 10. The distribution in the z''-direction, parallel to the rotation axis, has a full width to half maximum of 6000 au, and a total extent of 12000 au.

Table 3. Parameters of kinematic model.

Parameter	Search Range	Best fit
$V_{\rm exp}$	15–32 km s^{-1}	21.0$\pm$3.5 km s^{-1}
$V_{\rm z0}$	8–10 km s^{-1}	9.0$\pm$0.5 km s^{-1}
$V_{\rm rot}$	1–5 km s^{-1}	2.9$\pm$0.9 km s^{-1}
α	0–180°	46°$\pm$22°
β	0–90°	48°$\pm$19°

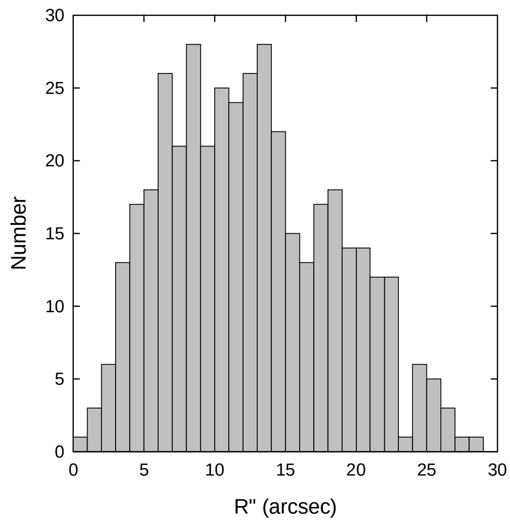

Figure 10. Radial distribution of the 1665-MHz OH masers about the disc rotation axis, determined using the kinematic model (Section 4.1).

The best-fitting expansion velocity is similar to that of the 'low-velocity outflow' seen in H_2O masers (Genzel et al., 1981). Solid body rotation becomes the dominant motion beyond a distance of 3240 au from the centre (a distance corresponding to 7.2 arcsec). Rotation is therefore the dominant motion for most of the system of OH masers, with however a significant component of expansion. The rotational period in our model is 760 yr, while the expansion timescale varies from $\sim$300 yr for the inner edge of the maser cavity to $\sim$3000 yr for the masers most distant from the expansion centre.

Most of the Orion nebula HH–objects are found at the tips of the H_2 'fingers' in the bipolar outflow shown in Fig. 6 and appear to have their origin in a newly created massive star that gives rise to the infrared source IRc 2 in the 10^5 $L_\odot$ Orion-BN/KL nebula in the OMC–1 cloud core. It has also been suggested that a minority of the prominent HH–objects have their origin in the neighbouring star forming region OMC–1S (Smith et al. 2004). However, excluding these few, Doi, O'Dell & Hartigan (2002) have used HST proper-motion measurements of the global expansion of the system of Orion HH–objects to demonstrate that the bipolar outflow is of Hubble type, i.e. the flow velocity is proportional to distance from the expansion centre. The bipolar flow therefore consists of 'bullets' all ejected around a 1000 yr ago in a single explosive event. Thus the expansion timescales determined for the OH masers bracket this H_2 timescale. These results suggest that the OH maser disc acquired its expansional motions in the same event that produced the H_2 bullets and the HH–objects found at the tips of the H_2 'fingers' in the bipolar outflow shown in Fig. 7.

The orientation of the rotation axis determined here agrees with that of the molecular outflow traced in CO and H_2 (e.g. Chernin & Wright 1996; Kaifu et al. 2000). It also coincides with the direction of the proper motions of source I and BN, and is close to the large-scale magnetic field direction inferred from far-infrared and submillimetre polarization (Schleuning 1998 and references therein).

We note that the velocities of order 20 km s^{-1} implied by our kinematic model correspond to proper motions $\sim$9 mas yr^{-1}, which could be measured by MERLIN within ten years.

4.2 The Nature of Stream A and Arc B

The major streams or arcs found in Orion-BN/KL have angular sizes greater than 5 arcsec, corresponding to projected sizes of at least 2250 au, which are almost unprecedented for interstellar OH masers. Stream A has no obvious counterpart in the infrared. However it points in the direction of the dominant infrared source BN, in the direction of the radio proper motions of BN and source I. Stream A has the appearance of a vapour trail that has formed in the wake of the runaway star BN. From the proper motion of BN and the projected separation from the Northern tip of Stream A we can infer a timescale of 200 yr. This may correspond to a cooling time, a formation time for OH, or a time for population inversion to be established following the passage of BN.

Fig. 1 shows that the proper motions of BN and sources I and n project back to a position on the sky near the base of Stream A, in a region largely clear of OH masers. This position is significantly displaced $\sim$4 arcsec Northwest of the centre of the OH maser torus. It has been suggested that BN and sources I and n originally belonged to a multiple stellar system that disintegrated $\sim$500 yr ago. The disintegration could have due to a close dynamical interaction, as suggested by Gómez et al. (in press), or it could have been due to a merger event that also produced the molecular outflow, as suggested by Bally & Zinnecker (2005). Alternatively, Tan (2004) has proposed that BN was ejected from the θ^1 Ori C system $\sim$4000 yr ago. Our data do not distinguish unambiguously between these possibilities. However the fact that the large-scale OH maser torus is centred on source I slightly favours Tan's scenario, with BN being a passing runaway from the θ^1 Ori C system.

The other large-scale feature Arc B encloses IRc6, which is one of the cooler mid-IR sources, with polarization that is consistent with external illumination and with no evidence of embedded bright stars (Shuping et al. 2004 and references therein). This suggests that Arc B might be associated with a photodissociation zone around IRc6. In further support of this there is strong emission from CH_3CH at the position of IRc6, implying densities of at least 10^6 cm^{-3} (Wilner, Wright & Plambeck 1996).

The large-scale maser structures found in Orion-BN/KL are similar in scale to OH maser structures recently reported in W3(OH). Wright et al. (2004a,b) noted several arcs of 18-cm masers, which they interpreted as propagating shocks. Harvey-Smith & Cohen (2005) found a low brightness filament of excited OH 4765-MHz emission stretching for $\sim$2200 au and clearly related in its morphology to some of the ground-state OH arcs at 18-cm wavelength. The structures seen in Orion are similar in linear scale. The individual maser spots in Stream A and Arc B are well separated on the sky for the most part, but are nevertheless likely to be simply the high-gain cores of an extended stream of maser

emission. The typical flux densities of ∼0.1 Jy correspond to brightness temperatures of at least $\sim 3\times 10^5$ K.

All these large-scale features in Orion and W3(OH) are relatively weak and therefore below the sensitivies of earlier surveys, for the most part. Deeper observations of other well-known OH maser sources are needed to establish just how common such features are.

4.3 The 1612-MHz Masers

The OH 1612-MHz masers have a more widespread distribution than the other OH masers, and different kinematics (Section 3.2). This suggests that they trace a region with different physical conditions. Gray, Field & Doel (1992) give the following conditions for strong 1612-MHz masers: molecular hydrogen density $n_{\rm H_2}$=6×10^6 cm^{-3}, $n_{\rm OH}$ 60 cm^{-3}, gas kinetic temperature $T_{\rm k}$=30 K, dust temperature at maser site $T_{\rm d}$ 30 K, external radiation field $T_{\rm x}$ 80 K and velocity shift ΔV 2.0 km s^{-1}. This is cooler than typical for OH masers, but is consistent with the location of these particular 1612-MHz masers further than normal from the main source of infrared luminosity. The velocity gradient needed for strong maser action is also consistent with the association of these masers with shocked gas in the molecular outflow (Section 3.3.2).

We note a further possible positional association between the 1612-MHz masers and the methanol 6.7-GHz masers recently discovered by Voronkov et al. (2005). In Fig. 11 we show the positions and velocities of the two species. There is a clear region of overlap centred around RA (J2000) = $05^{\rm h}35^{\rm m}14\overset{\rm s}{.}5$, Dec. (J2000) = $-05^\circ 22' 45\overset{''}{.}9$ and $V_{\rm lsr}$= +7.5 km s^{-1}. The 6.7-GHz positions have errors of ∼2 arcsec. It will be important to make 6.7-GHz measurements of higher precision to examine this correspondence more closely. The positions of 25-GHz masers from Johnston et al. (1997, 1992) are also shown in the figure for completeness. Only one of these falls in the region of interest. We note that there is no association with the OH mainline masers. This is consistent with the 25-GHz masers being class I masers, which are thought to be collisionally pumped (cf. Cragg et al. 2002).

The 6.7-GHz maser transition is the prototype class II maser, usually thought to be radiatively pumped. The 6.7-GHz masers in Orion are of therefore of interest because of their apparent association with 25-GHz masers. Voronkov et al. have considered the pumping requirements for the co-existence of both types of methanol maser and find that both types can occur simultaneously at low temperature (∼60 K) and low molecular hydrogen density ($\sim 10^5$ cm^{-3}). These conditions are not too dissimilar to those needed for strong 1612-MHz masers, as given earlier. In summary, it appears that in Orion we may have the first examples of both methanol class II and OH ground state masers located far from the main source of infrared luminosity, and associated instead with the interaction between the molecular outflow and the surrounding gas.

4.4 Proplyd region

The proplyds originally designated LV 1–6 within the Orion Trapezium cluster are those most likely to exhibit maser

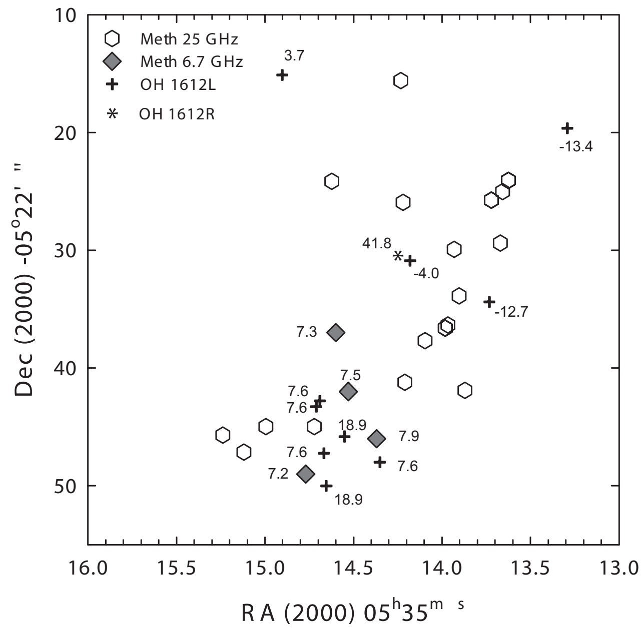

Figure 11. Positions and velocities of OH 1612-MHz masers (this paper) compared with those of the newly discovered methanol 6.7-GHz masers (Voronkov et al. 2005). Positions of 25-GHz methanol masers from Johnston et al. (1997) and Johnston et al. (1992) are also shown. The radial velocities at 25 GHz are confined to a narrow range of 7–10 km s^{-1}.

emission for they are irradiated by the intense field of the O6.5 star θ^1 Ori C. Of these LV 1, now resolved as a binary proplyd (168–326 NW & SE) by O'Dell & Wen (1994), and LV 2 (proplyd 167-317 of O'Dell & Wen 1994) have been most intensively observed (Graham et al. 2002; Henney et al. 2002 respectively).

The 8×10^{14} cm radius LV 2 was shown by Henney et al. (2002) to be irradiated by a flux of 3×10^4 cm^{-2} s^{-1} Lyman photons. These produce an ionised skin with a measured electron density $n_e = 2.6\times 10^6$ cm^{-3} on the surface of a neutral disk or cocoon which envelopes the low mass YSO (Meaburn 1988). From 1.3-mm interferometric observations Bally et al. (1998b) deduce an upper limit to the mass of molecular hydrogen in this neutral component of ∼0.015 $M_\odot$ to give an H_2 density of $n_o \leq 4.2\times 10^9$ cm^{-3}. On the other hand, simple pressure balance between the ionised and neutral gas with temperatures of $T_e = 10^4$ K and $T_o = 10^3$ K would give $n_o \approx 5.2\times 10^9$ cm^{-3}.

OH masers have yet to be found in regions of purely low-mass star-formation. However, it is this dense, circumstellar molecular gas around proplyds, stimulated by photons from θ^1Ori C, that is the potential source of any maser emission. We would expect to find OH masers at a distance of $\sim 7\times 10^{17}$cm from an O6.5 star (cf. Baart & Cohen 1985). However, if Keplerian motion around the YSO occurs in this neutral cocoon it will have a rotational velocity of 4 km s^{-1} at its outer edge with higher velocities towards the centre (proportional to radius$^{-1/2}$). In these circumstances the velocity coherence required for strong maser amplification will occur over a path length that is much smaller than the overall radius of the proplyd. This, together with possible chem-

ical effects (Section 3.5), could explain our non-detection of OH masers in this region.

5 CONCLUSIONS

The distribution of OH masers in the Orion-BN/KL region is far more extensive than previously realized, covering a region of 30 arcsec extent and a radial velocity range from –13 to +42 km s^{-1}. The bulk of the emission can be modelled in terms of a rotating and expanding torus, centred on IRc2 or radio source I, with an inner cavity of ∼1300 au radius. The rotation axis has the same position angle and inclination to the line-of-sight as the molecular outflow and the large scale magnetic field inferred from mm- and submm-polarization (Section 4.1). The dynamical timescale is similar to that of the explosive event that produced the widespread shocked H_2 emission. It is likely that the OH masers trace the interaction between the low-velocity molecular outflow and the molecular hot core, and that they acquired their expansional motions in the same event that produced the outflow.

Of particular interest is a string of masers, Stream A, at ∼21 km s^{-1}, that extends at position angle ∼45°between IRc2 and BN, in the direction of the radio proper motions of these two dominant sources. We suggest that Stream A may have appeared, like a vapour trail, in the wake of the runaway star BN. The proper motions of BN and sources I and n project back to the base of Stream A (Fig. 1), ∼4 arcsec Northwest of the centre of the OH maser torus, a position that is largely devoid of masers.

The 1612-MHz masers have a more widespread distribution than the other OH masers, with kinematics that are more like those of the H_2O masers associated with the outflow. Many of these 1612-MHz masers are spatially associated with fingers of shocked H_2 emission (Fig. 7). These OH masers are thought to require relatively low gas and dust temperatures for their inversion (Section 4.3). Apart from the OH 1612-MHz masers, the other OH masers have complementary distributions and kinematics to the H_2O masers (Figs. 1–4), with essentially no overlap. OH is also spatially and kinematically distinct from the class I methanol 25-GHz masers. A possible correspondence between OH 1612-MHz and class II methanol 6.7-GHz masers reported by Voronkov et al. (2005) requires further study at higher angular resolution.

The magnetic field strength in the OH maser regions ranges from 1.8 to 16.3 mG, with a possible field reversal (Section 3.4).

A search for OH masers associated with the proplyds around θ^1 Ori C yielded only upper limits, which may indicate a low OH abundance in this more evolved region.

ACKNOWLEDGMENTS

We thank the anonymous referee for helpful comments and in particular for drawing our attention to the paper by Gómez et al. We thank Busaba Hutawarakorn for assistance with the data reduction, Ralph Shuping for providing a high resolution version of the Keck image in Fig. 5, and Masa Hayashi for providing high resolution Subaru data used in Figs. 6 and 7. NG gratefully acknowledges the Thai Astronomy Co-operative Research Network for their support. MERLIN is a national facility operated by the University of Manchester on behalf of PPARC.

REFERENCES

Allen D.A., Burton M. G., 1993, Nat, 363, 54.
Baart E. B., Cohen R. J., 1985, MNRAS, 213, 641
Bally J., Sutherland R. S., Devine D., Johnstone D., 1998a, AJ, 116, 293.
Bally J., Testi L., Sargent A., Carlstrom J., 1998b, AJ, 116, 854.
Bally J., Zinnecker H., 2005, AJ, 129, 2281.
Blaskiewicz A., Szymczak M., Cohen R. J., Richards A. M. S., 2005, MNRAS, 361, 623.
Chapman J. M., Cohen R. J., 1986, MNRAS, 220, 513
Chernin L. M., Wright M. C. H., 1996, ApJ, 467, 676
Churchwell E., Felli M., Wood D. O. S., Massi M., 1987, ApJ, 321, 516.
Cragg D.M., Sobolev A.M., Godfrey P.D., 2002, MNRAS, 331, 521
Doi T., O'Dell C. R., Hartigan P. 2002, AJ, 124, 445.
Gasiprong N., Cohen R. J., Hutawarkorn B., 2002, MNRAS, 336, 47
Gaume R. A., Wilson T. L., Vrba F. J., Johnston K. J., Schmid-Burgk J., 1998, ApJ, 493, 940
Genzel R., Reid M. J., Moran J. M., Downes D., 1981, ApJ, 244, 884
Gómez L., Rodríguez L. F., Loinard L., Lizano S., in press, astro-ph/0509201.
Graham M. F., Meaburn J., Garrington, S. T., O'Brien T. J., Henney W. J., O'Dell C. R., 2002, ApJ, 570, 222.
Graham M. F., Meaburn J., Redman, M. P., 2003, MNRAS, 343, 419
Gray M.D., Field D., Doel R.C., 1992, A&A, 262, 555
Greenhill L. J., Gwinn C. R., Schwartz C., Moran J. M., Diamond P. J., 1998, Nat, 396, 650
Hansen S. S., Johnston K. J., 1983, ApJ, 267, 625
Harvey-Smith L., Cohen R. J., 2005, MNRAS, 356, 637
Hayward T. L., Houck J. R., Miles J. W., 1994, ApJ, 433, 157
Henney W. J., O'Dell C. R., Meaburn J., Garrington S.T., López J. A., 2002, ApJ, 566, 315.
Hillenbrand L. A., Carpenter J. M., 2000, ApJ, 540, 236
Hutawarakorn B., Cohen R. J., 2005, MNRAS, 357, 338
Johnston K. J., Migenes V., Norris R. P., 1989, ApJ, 341, 847,
Johnston K. J., Gaume R. A., Stolovy S., Wilson T. L., Walmsley C. M., Menten K. M., 1992, ApJ, 385, 232
Johnston K. J., Gaume R. A., Wilson T. L., Nguyen H. A., Nedoluha G. E., 1997, ApJ, 490, 758
Kaifu N., et al., 2000, PASJ, 52, 1
Laques P., Vidal J. P., 1979, AA, 73, 97.
McCaughrean M. J., Stauffer J. R., 1994, AJ, 108, 1382.
Meaburn J. 1988, MNRAS, 233, 791.
Menten K. M., Reid M. J., 1995, ApJ, 445, L157
Motohara K., et al. 1998, Proc. SPIE, Vol. 3354, 659-667, Infrared and Astronomical Instrumentation, ed. A. M. Fowler (International Society for Optical Engineering, USA)
Norris R. P., 1984, MNRAS, 207, 127
O'Dell C. R., Wen, Z., Hu, X 1993, ApJ, 410, 696.
O'Dell C. R., Wen, Z. 1994, ApJ, 436, 194.
O'Dell C. R., Wong K., 1996, AJ, 111, 846
Plambeck R. L., Wright M. C. H., Mundy L. G., Looney L. W., 1995, ApJ, 455, L189
Price W. L., 1976, Computer J., 20, 367
Reid M. J., Schneps M. H., Moran J. M., Gwinn C. R., Genzel R., Downes D., Rönnäng, 1988, ApJ, 330, 809

Rodgers S. D., Charnely S. B., 2001, ApJ, 546, 324
Rodríguez L. F., Poveda A., Lizano S., Allen, C., 2005, ApJ, 627, L65
Schleuning D. A., 1998, ApJ, 493, 811
Scoville N., Kleinmann S. G., Hall D. N. B., Ridgway S. T., 1983, ApJ, 275, 201.
Shuping, R. Y., Morris, M., Bally, J., 2004, AJ, 128, 363
Smith N., Bally J., Shuping, R. Y., Morris M., Hayward T. L., 2004, ApJ, 610, L117.
Smith N., Bally J., Shuping, Y., Morris M. and Kassis M., 2005, AJ, 130, 1763.
Tan, J. C., 2004, APJ, 607, L47.
Voronkov M. A., Sobolev A. M., Ellingsen S. P., Ostrovskii A. B., 2005, MNRAS, 362, 995.
Wilner D. J., Wright M. C. H., Plambeck R. L., ApJ, 422, 642
Wilson, T. L., Gaume, R. A., Gensheimer, P., Johnston, K. J., 2000, ApJ, 538, 665.
Wright M. C. H., Plambeck R. L., Lundy L. G., Looney L. W., 1995, ApJ, 455, L185.
Wright M. C. H., Plambeck R. L., Wilner D. J., 1996, ApJ, 469, 216.
Wright M. M., Gray M. D., Diamond P. J., 2004a, MNRAS, 350, 1253
Wright M. M., Gray M. D., Diamond P. J., 2004b, MNRAS, 350, 1272
Zapata, L. A., Rodríguez, L. F., Kurtz, S. E., O'Dell, C. R., 2004, AJ, 17, 2252

Table 1. OH 1.6-GHz Masers in Orion-BN/KL.

Transition	Feature No.	Velocity (km s^{-1})	RA(1950) 05^h32^m ^{s}	Dec(1950) –5°:24′:″	RA(2000) 05^hh35^m ^{s}	Dec(2000) –5°:22′:″	Intensity (Jy $beam^{-1}$)
1612L	1	–13.41	45.8137	13.153	13.2911	19.624	0.20
	2	–12.68	46.2592	27.890	13.7318	34.393	0.11
	3	–3.97	46.7062	24.344	14.1800	30.880	0.20
	4	3.66	47.4242	08.524	14.9030	15.112	0.11
	5	7.64	46.8839	41.471	14.3521	48.019	0.09
	6	7.64	47.1993	40.678	14.6677	47.249	0.12
	7	7.64	47.2210	36.224	14.6908	42.797	0.12
	8	7.64	47.2417	36.726	14.7114	43.300	0.17
	9	18.93	47.0810	39.263	14.5499	45.826	0.08
	10	18.93	47.1858	43.452	14.6533	50.022	0.13
1612R	1	41.80	46.7773	24.354	14.2510	30.895	0.12
1665L	1	–10.70	46.6328	22.505	14.1072	29.035	0.14
	2	–10.42	46.7912	22.176	14.2656	28.718	0.24
	3	–9.64	46.8095	22.013	14.2840	28.557	0.14
	4	–9.64	47.0398	22.993	14.5139	29.553	0.34
	5	–9.32	46.4472	22.867	13.9214	29.384	0.17
	6	–9.11	46.7827	21.337	14.2574	27.878	0.13
	7	–8.59	46.8077	23.509	14.2817	30.052	0.27
	8	–8.24	46.4518	22.571	13.9261	29.088	0.12
	9	–8.02	46.7338	21.544	14.2084	28.082	0.17
	10	–7.88	46.6340	23.458	14.1080	29.989	0.24
	11	–7.88	46.7335	21.526	14.2082	28.064	0.17
	12	–7.88	46.6316	22.036	14.1061	28.566	0.20
	13	–7.53	46.9440	20.729	14.4189	27.282	0.10
	14	–7.53	46.9255	20.468	14.4005	27.019	0.11
	15	–7.36	46.8692	20.569	14.3442	27.116	0.90
	16	–7.36	46.9485	20.810	14.4234	27.364	0.13
	17	–6.89	46.7149	21.956	14.1894	28.493	0.16
	18	–6.83	46.7282	20.943	14.2031	27.480	0.12
	19	–6.61	46.7719	21.301	14.2466	27.842	0.19
	20	–6.13	46.7809	20.927	14.2558	27.468	0.17
	21	–6.13	46.7442	20.854	14.2191	27.392	0.10
	22	–5.83	46.8968	23.735	14.3707	30.284	0.73
	23	–5.77	46.8065	21.846	14.2811	28.389	0.10
	24	–5.77	46.7768	21.284	14.2516	27.825	0.14
	25	–5.77	46.9090	23.745	14.3829	30.295	0.42
	26	–5.69	46.7619	20.790	14.2368	27.329	0.26
	27	–5.42	46.9295	20.677	14.4044	27.229	0.10
	28	–5.42	46.9134	23.784	14.3873	30.335	0.69
	29	–5.42	46.9386	33.358	14.4094	39.910	0.08
	30	–4.37	46.8096	21.692	14.2842	28.236	0.09
	31	–4.02	46.7662	21.057	14.2410	27.597	0.14
	32	–3.89	47.1898	17.315	14.6658	23.886	0.28
	33	–3.31	46.5602	21.601	14.0348	28.126	0.16
	34	–2.96	46.9105	19.907	14.3857	26.458	0.15
	35	–2.96	46.5629	21.625	14.0375	28.150	0.13
	36	–2.61	47.0183	33.522	14.4890	40.080	0.10
	37	–2.26	46.7894	20.575	14.2644	27.117	0.21
	38	–1.91	46.8197	20.397	14.2948	26.941	0.22
	39	–1.56	46.6744	21.334	14.1491	27.867	0.35
	40	–1.56	46.8823	20.338	14.3574	26.887	0.12
	41	–1.38	46.9594	23.707	14.4334	30.261	0.44

Table 1. OH 1.6-GHz Masers in Orion-BN/KL, continued.

Transition	Feature No.	Velocity (km s^{-1})	RA(1950) 05^h32^m ^{s}	Dec(1950) –5°:24′: ″	RA(2000) 05^hh35^m ^{s}	Dec(2000) –5°:22′: ″	Intensity (Jy $beam^{-1}$)
1665L	42	–0.85	46.8218	20.452	14.2968	26.997	0.42
	43	0.30	46.8021	23.549	14.2761	30.092	0.58
	44	0.37	47.1572	19.302	14.6326	25.870	0.29
	45	0.46	46.9636	23.523	14.4376	30.077	1.84
	46	1.14	46.9246	22.479	14.3989	29.031	0.24
	47	1.61	46.9754	23.672	14.4493	30.228	0.13
	48	1.61	46.9424	23.138	14.4165	29.691	0.13
	49	1.61	46.9523	25.187	14.4258	31.740	0.13
	50	1.84	46.9463	23.766	14.4202	30.319	6.77
	51	2.99	46.9400	22.603	14.4142	29.156	1.25
	52	3.37	46.9964	23.444	14.4704	30.001	0.12
	53	3.37	46.5059	20.795	13.9808	27.317	0.11
	54	3.65	46.8365	20.701	14.3114	27.246	0.26
	55	3.70	46.9524	23.681	14.4263	30.235	1.25
	56	3.72	46.4051	20.615	13.8801	27.129	0.11
	57	3.72	46.3534	21.314	13.8281	27.825	0.10
	58	3.72	46.7119	20.664	14.1868	27.201	0.19
	59	3.89	46.5796	21.329	14.0543	27.855	0.57
	60	4.03	46.6630	20.911	14.1379	27.444	0.51
	61	4.07	46.5423	21.241	14.0171	27.765	0.14
	62	4.63	46.7483	20.876	14.2232	27.415	1.22
	63	4.69	46.6243	21.026	14.0991	27.555	0.35
	64	4.77	46.9233	23.267	14.3974	29.819	0.16
	65	4.77	46.6881	20.622	14.1631	27.157	0.15
	66	4.77	46.9581	22.943	14.4323	29.497	0.12
	67	4.77	46.5770	21.333	14.0518	27.859	0.10
	68	4.77	46.4888	21.276	13.9636	27.796	0.10
	69	4.77	46.7341	20.653	14.2091	27.191	0.14
	70	4.94	46.9280	24.075	14.4018	30.627	13.19
	71	5.58	46.9628	22.884	14.4370	29.438	1.35
	72	5.83	46.6159	20.657	14.0909	27.186	0.11
	73	5.83	46.3649	18.674	13.8405	25.185	0.10
	74	5.95	46.6308	21.075	14.1056	27.605	0.17
	75	6.53	46.9632	22.822	14.4374	29.376	0.13
	76	6.64	46.4056	18.590	13.8812	25.104	0.56
	77	6.66	46.9574	23.654	14.4313	30.207	3.54
	78	6.88	47.4785	19.472	14.9538	26.063	0.11
	79	7.29	46.9105	24.319	14.3842	30.870	2.03
	80	7.42	46.9717	20.929	14.4466	27.484	0.23
	81	7.59	46.5247	20.806	13.9996	27.329	0.12
	82	7.71	46.6617	29.943	14.1337	36.475	0.20
	83	7.70	46.8017	24.012	14.2755	30.555	0.26
	84	7.93	47.4563	19.610	14.9316	26.200	0.55
	85	8.36	46.8554	25.968	14.3286	32.514	0.31
	86	8.91	46.7967	24.106	14.2705	30.648	2.99
	87	8.98	46.9087	24.312	14.3824	30.863	1.57
	88	8.99	46.9060	22.794	14.3802	29.344	0.11
	89	9.06	46.9558	20.654	14.4307	27.207	0.40
	90	9.70	47.5408	20.189	15.0158	26.786	0.33
	91	9.81	46.5539	20.811	14.0288	27.336	0.37
	92	10.75	47.0620	24.863	14.5356	31.424	0.21
	93	10.75	47.3672	21.696	14.8418	28.279	0.14

Table 1. OH 1.6-GHz Masers in Orion-BN/KL, continued.

Transition	Feature No.	Velocity (km s^{-1})	RA(1950) $05^h32^m\ ^s$	Dec(1950) $-5°:24':''$	RA(2000) $05^h h35^m\ ^s$	Dec(2000) $-5°:22':''$	Intensity (Jy $beam^{-1}$)
1665L	94	11.10	46.7601	30.912	14.2317	37.452	0.13
	95	11.19	47.4566	18.226	14.9322	24.816	0.29
	96	11.21	47.3960	18.029	14.8717	24.615	0.38
	97	11.59	46.9193	23.131	14.3934	29.682	0.26
	98	11.89	47.4229	21.920	14.8973	28.508	2.17
	99	12.16	47.0610	24.863	14.5346	31.424	0.25
	100	12.55	46.9741	23.885	14.4479	30.440	2.50
	101	12.86	47.0105	21.980	14.4849	28.538	0.10
	102	12.94	46.9106	23.520	14.3846	30.071	0.50
	103	13.21	47.0528	21.892	14.5273	28.453	0.11
	104	13.21	46.9949	21.645	14.4695	28.202	0.19
	105	13.54	46.9486	23.990	14.4225	30.543	4.66
	106	13.56	46.9987	21.742	14.4733	28.299	0.37
	107	13.92	46.7596	19.790	14.2348	26.330	0.15
	108	15.15	46.7672	19.970	14.2424	26.510	0.10
	109	15.32	46.7762	30.758	14.2479	37.298	0.11
	110	15.67	46.7458	19.896	14.2210	26.434	0.14
	111	15.73	47.1206	22.445	14.5949	29.010	0.56
	112	15.81	47.0033	21.966	14.4778	28.523	0.33
	113	15.90	47.3826	21.547	14.8572	28.131	1.62
	114	16.23	47.0147	22.161	14.4891	28.719	0.69
	115	16.50	47.3545	21.873	14.8290	28.455	0.23
	116	16.86	47.3909	20.129	14.8660	26.714	0.15
	117	17.03	47.1812	21.727	14.6557	28.297	0.20
	118	17.08	47.3752	21.588	14.8498	28.172	0.15
	119	17.08	47.0071	21.910	14.4816	28.468	0.13
	120	17.22	47.1108	21.999	14.5853	28.564	0.18
	121	17.43	47.1021	22.817	14.5764	29.381	0.13
	122	17.43	47.3406	22.604	14.8149	29.185	0.12
	123	17.43	47.0877	22.617	14.5620	29.180	0.12
	124	17.61	47.2131	22.777	14.6873	29.349	0.28
	125	17.78	47.0585	22.618	14.5328	29.179	0.13
	126	17.78	47.1081	22.726	14.5824	29.291	0.14
	127	17.78	47.3509	22.000	14.8254	28.582	0.13
	128	17.78	47.1612	22.569	14.6355	29.137	0.10
	129	17.78	47.1809	21.706	14.6555	28.276	0.30
	130	17.78	47.2869	22.111	14.7614	28.688	0.11
	131	17.78	47.4061	21.989	14.8806	28.575	0.10
	132	17.91	47.0200	21.993	14.4945	28.552	0.42
	133	18.13	47.3239	21.992	14.7984	28.572	0.10
	134	18.13	47.1849	23.365	14.6589	29.936	0.24
	135	18.13	46.8631	20.019	14.3382	26.566	0.11
	136	18.13	47.0591	22.609	14.5334	29.170	0.11
	137	18.13	47.1708	23.045	14.6449	29.614	0.28
	138	18.13	47.2031	22.800	14.6773	29.372	0.15
	139	18.37	47.1359	22.256	14.6103	28.823	1.91
	140	18.45	47.3202	22.860	14.7944	29.441	0.74
	141	18.49	47.3692	21.736	14.8438	28.319	0.10
	142	18.49	47.2276	22.656	14.7019	29.229	0.14
	143	18.68	47.2708	23.175	14.7449	29.752	0.17
	144	18.77	47.1887	23.174	14.6628	29.745	0.38
	145	18.84	47.2506	23.248	14.7247	29.823	0.10

Table 1. OH 1665-MHz Masers in Orion-BN/KL, continued.

Transition	Feature No.	Velocity (km s^{-1})	RA(1950) 05^h32^m s	Dec(1950) –5°:24′: ″	RA(2000) 05^hh35^m s	Dec(2000) –5°:22′: ″	Intensity (Jy $beam^{-1}$)
1665L	146	18.84	47.0446	22.294	14.5190	28.854	0.10
	147	19.19	47.2460	23.949	14.7199	30.524	0.10
	148	19.19	46.9805	21.779	14.4551	28.335	0.11
	149	19.28	47.3395	22.238	14.8139	28.820	1.13
	150	19.30	47.1008	22.783	14.5750	29.347	0.41
	151	19.39	47.1682	22.963	14.6424	29.532	0.73
	152	19.49	47.2982	22.553	14.7724	29.132	1.38
	153	19.54	47.1921	18.773	14.6676	25.344	0.82
	154	19.54	47.2170	23.168	14.6911	29.740	0.12
	155	19.72	47.1863	22.905	14.6604	29.476	0.65
	156	19.89	47.3449	22.840	14.8191	29.422	0.11
	157	20.00	47.2990	22.998	14.7731	29.576	0.39
	158	20.06	47.2813	22.322	14.7557	28.900	1.34
	159	20.22	47.2210	23.460	14.6950	30.033	0.38
	160	20.24	47.1731	22.703	14.6474	29.273	0.24
	161	20.24	47.3741	21.408	14.8487	27.992	0.20
	162	20.24	47.1283	22.622	14.6026	29.188	0.10
	163	20.25	47.3230	22.147	14.7975	28.728	0.35
	164	20.51	46.8612	20.236	14.3363	26.783	0.22
	165	20.60	47.1461	22.794	14.6203	29.362	0.09
	166	20.60	46.6794	19.235	14.1548	25.769	0.11
	167	20.60	47.1822	23.165	14.6563	29.735	0.10
	168	20.60	47.3399	21.344	14.8146	27.926	0.12
	169	20.81	47.2581	22.024	14.7326	28.600	0.52
	170	20.95	47.3357	20.783	14.8106	27.364	0.12
	171	20.95	47.2488	22.793	14.7230	29.368	0.11
	172	21.10	47.2681	23.215	14.7421	29.792	0.31
	173	21.10	46.7578	18.778	14.2334	25.318	0.12
	174	21.11	46.8273	19.902	14.3024	26.446	0.11
	175	21.19	47.2243	22.961	14.6984	29.534	0.29
	176	21.28	47.3091	21.994	14.7836	28.574	0.78
	177	21.30	47.0599	22.222	14.5343	28.784	0.11
	178	21.30	47.0945	22.299	14.5689	28.863	0.11
	179	21.30	46.8812	20.791	14.3561	27.340	0.14
	180	21.43	47.1741	22.606	14.6484	29.176	0.24
	181	21.65	47.0019	21.539	14.4766	28.096	0.10
	182	21.66	47.2872	21.697	14.7618	28.274	0.42
	183	21.98	46.8077	19.522	14.2830	26.065	0.18
	184	22.00	46.7810	19.400	14.2564	25.941	0.11
	185	22.06	47.1652	21.292	14.6399	27.861	0.58
	186	22.15	47.2621	21.690	14.7366	28.266	0.23
	187	22.21	46.7510	18.649	14.2266	25.188	0.32
	188	22.35	47.1823	22.474	14.6566	29.045	0.11
	189	22.35	47.2012	22.210	14.6756	28.782	0.10
	190	22.35	47.2252	21.153	14.6999	27.726	0.10
	191	22.45	47.3097	21.363	14.7844	27.942	0.22
	192	22.52	46.7363	18.380	14.2120	24.918	0.11
	193	22.52	47.1626	21.569	14.6372	28.137	1.16
	194	22.68	46.7764	19.147	14.2518	25.687	0.20
	195	22.70	47.2990	22.012	14.7734	28.591	0.10
	196	22.70	47.3204	21.683	14.7950	28.263	0.12
	197	22.89	47.2768	21.329	14.7515	27.906	0.24

Table 1. OH 1.6-GHz Masers in Orion-BN/KL, continued.

Transition	Feature No.	Velocity (km s^{-1})	RA(1950) 05$^{\rm h}$32$^{\rm m}$ $^{\rm s}$	Dec(1950) –5°:24′: ″	RA(2000) 05$^{\rm h}$h35$^{\rm m}$ $^{\rm s}$	Dec(2000) –5°:22′: ″	Intensity (Jy beam^{-1})
1665L	198	23.45	47.3606	19.136	14.8360	25.719	0.14
	199	23.76	47.0703	21.506	14.5449	28.068	0.09
	200	25.52	47.1255	20.913	14.6003	27.479	0.12
	201	30.27	47.0935	20.382	14.5685	26.946	0.27
	202	37.12	46.9894	20.319	14.4644	26.876	0.11
	203	38.34	46.9856	20.301	14.4607	26.857	0.17
	204	38.53	47.5898	14.835	15.0666	21.435	0.10
1665R	1	–10.64	46.7892	22.184	14.2636	28.725	0.15
	2	–8.94	46.7760	21.434	14.2507	27.975	0.13
	3	–8.59	46.8107	23.575	14.2847	30.118	0.25
	4	–8.59	46.8138	21.872	14.2884	28.415	0.11
	5	–8.59	46.8852	19.533	14.3605	26.082	0.10
	6	–8.08	46.4489	22.618	13.9232	29.135	0.19
	7	–8.04	46.9381	20.614	14.4131	27.167	0.16
	8	–7.88	46.6323	22.058	14.1068	28.589	0.12
	9	–7.88	46.9518	20.971	14.4266	27.525	0.12
	10	–7.53	46.8734	24.560	14.3471	31.108	0.16
	11	–7.53	46.8974	20.259	14.3724	26.809	0.13
	12	–7.27	46.8497	24.540	14.3234	31.086	1.72
	13	–7.00	46.9321	20.761	14.4070	27.313	0.72
	14	–6.83	46.7781	21.029	14.2529	27.570	0.12
	15	–6.55	46.6520	22.005	14.1265	28.537	0.26
	16	–6.48	46.7726	21.349	14.2473	27.889	0.20
	17	–6.48	46.7973	21.298	14.2720	27.841	0.10
	18	–6.23	46.6608	23.428	14.1349	29.960	1.18
	19	–5.77	46.8957	23.757	14.3696	30.307	0.24
	20	–5.77	46.7760	21.290	14.2507	27.831	0.11
	21	–5.67	46.9149	23.815	14.3888	30.365	0.48
	22	–5.42	46.5014	11.572	13.9793	18.093	0.09
	23	–4.25	47.0269	24.013	14.5007	30.572	0.23
	24	–3.89	46.6230	21.806	14.0976	28.336	0.18
	25	–3.52	46.7739	20.874	14.2488	27.414	0.42
	26	–3.31	46.5598	21.664	14.0344	28.189	0.26
	27	–3.31	46.4710	21.594	13.9456	28.113	0.11
	28	–3.31	47.6469	23.613	15.1208	30.217	0.10
	29	–1.91	46.8620	20.278	14.3370	26.825	0.20
	30	–1.35	46.9597	23.737	14.4336	30.291	0.93
	31	–0.50	47.5735	25.373	15.0469	31.971	0.12
	32	0.02	47.1037	21.252	14.5785	27.816	1.82
	33	0.55	46.8028	23.592	14.2767	30.135	0.15
	34	0.72	46.9623	23.565	14.4363	30.119	3.03
	35	1.15	46.7232	20.962	14.1980	27.499	0.30
	36	1.87	46.9477	23.778	14.4216	30.331	4.29
	37	1.96	46.9203	23.109	14.3944	29.660	0.10
	38	1.96	46.9669	24.141	14.4407	30.696	0.10
	39	2.31	46.7483	21.446	14.2230	27.985	0.10
	40	2.34	46.6527	20.863	14.1275	27.395	0.28
	41	2.43	46.7296	20.860	14.2044	27.397	0.27
	42	2.43	46.7989	23.565	14.2729	30.108	1.48
	43	2.44	46.7811	21.544	14.2557	28.085	0.24
	44	2.90	46.5691	21.459	14.0438	27.984	0.19
	45	3.02	46.9402	22.635	14.4144	29.188	0.29

Table 1. OH 1.6-GHz Masers in Orion-BN/KL, continued.

Transition	Feature No.	Velocity (km s^{-1})	RA(1950) 05^{h}32^{m} ^{s}	Dec(1950) –5°:24′: ″	RA(2000) 05^{h}h35^{m} ^{s}	Dec(2000) –5°:22′: ″	Intensity (Jy beam^{-1})
1665R	46	3.53	46.7474	20.716	14.2223	27.254	1.01
	47	3.61	46.6689	20.895	14.1438	27.428	0.39
	48	3.72	46.7300	20.675	14.2049	27.213	0.23
	49	4.07	46.5933	21.349	14.0680	27.877	0.78
	50	4.07	46.5446	21.273	14.0194	27.797	0.21
	51	4.24	46.8052	23.576	14.2792	30.119	0.18
	52	4.42	46.7489	20.825	14.2238	27.364	0.21
	53	4.77	46.6189	21.236	14.0937	27.765	0.19
	54	5.03	46.7662	20.640	14.2412	27.180	1.01
	55	5.13	47.0036	23.137	14.4777	29.694	0.13
	56	5.13	47.0114	21.280	14.4861	27.837	0.10
	57	5.42	46.9331	24.058	14.4069	30.610	13.32
	58	5.48	46.9861	22.727	14.4603	29.283	0.13
	59	5.48	46.9150	22.140	14.3895	28.691	0.11
	60	5.48	46.9950	21.363	14.4697	27.920	0.12
	61	5.48	46.9345	23.217	14.4086	29.769	0.11
	62	5.60	46.9629	22.917	14.4371	29.472	1.97
	63	5.63	47.1711	34.641	14.6414	41.210	0.13
	64	5.66	47.1858	34.679	14.6562	41.249	0.15
	65	5.83	46.6880	20.712	14.1630	27.246	0.12
	66	5.83	46.3557	19.353	13.8311	25.863	0.12
	67	6.18	46.6603	20.783	14.1352	27.316	0.12
	68	6.18	46.4246	18.394	13.9003	24.909	0.12
	69	6.18	46.8949	20.286	14.3700	26.836	0.29
	70	6.29	46.3697	18.686	13.8453	25.197	0.30
	71	6.53	46.9588	22.910	14.4330	29.464	0.14
	72	6.61	46.7039	20.616	14.1789	27.151	1.09
	73	6.63	46.4055	18.617	13.8811	25.131	0.52
	74	6.88	47.4773	19.497	14.9526	26.089	0.10
	75	6.88	47.4471	19.446	14.9224	26.035	0.11
	76	7.01	47.2481	35.460	14.7182	42.034	0.20
	77	7.11	46.6565	20.807	14.1314	27.339	0.49
	78	7.12	46.7840	24.318	14.2577	30.860	0.32
	79	7.23	46.9036	24.377	14.3773	30.927	3.04
	80	7.43	47.4634	19.557	14.9387	26.148	0.55
	81	7.59	46.5732	20.572	14.0482	27.098	0.10
	82	7.59	46.7991	24.012	14.2729	30.554	0.11
	83	7.59	46.5521	21.000	14.0269	27.525	0.14
	84	7.73	46.4607	35.073	13.9310	41.591	0.88
	85	7.94	46.6746	20.700	14.1495	27.233	0.10
	86	7.94	46.6647	29.883	14.1367	36.416	0.11
	87	8.63	47.4493	19.666	14.9245	26.255	0.22
	88	8.64	46.6916	29.404	14.1637	35.938	0.28
	89	8.64	46.8272	23.964	14.3011	30.508	0.10
	90	8.64	47.1435	21.659	14.6181	28.227	0.15
	91	8.79	47.3896	18.152	14.8653	24.737	0.15
	92	8.84	46.8000	24.518	14.2737	31.060	0.17
	93	8.99	47.6212	20.111	15.0962	26.713	0.11
	94	8.99	47.0118	23.011	14.4860	29.569	0.14
	95	8.99	46.6573	20.772	14.1322	27.304	0.12
	96	9.18	47.5979	19.677	15.0731	26.277	0.22
	97	9.34	47.5998	19.994	15.0749	26.594	0.10

Table 1. OH 1.6-GHz Masers in Orion-BN/KL, continued.

Transition	Feature No.	Velocity (km s^{-1})	RA(1950) 05^h32^m ^{s}	Dec(1950) –5°:24′: ″	RA(2000) 05^hh35^m ^{s}	Dec(2000) –5°:22′: ″	Intensity (Jy $beam^{-1}$)
1665R	98	9.34	47.0384	22.393	14.5127	28.953	0.12
	99	9.34	47.5797	19.486	15.0550	26.085	0.13
	100	9.49	46.8978	20.275	14.3729	26.825	0.14
	101	10.05	46.9781	22.586	14.4524	29.141	0.24
	102	10.70	46.7569	31.179	14.2284	37.718	0.34
	103	10.75	47.3695	21.663	14.8441	28.247	0.14
	104	10.79	47.0691	21.578	14.5437	28.140	1.26
	105	11.10	46.6243	20.873	14.0992	27.403	0.24
	106	11.10	47.4608	18.220	14.9365	24.810	0.12
	107	11.25	47.3932	18.070	14.8689	24.656	0.45
	108	11.81	47.3321	10.317	14.8104	16.898	0.12
	109	11.81	47.4134	23.297	14.8874	29.884	0.12
	110	11.81	47.4272	21.925	14.9017	28.512	1.46
	111	12.16	47.0128	21.766	14.4874	28.324	0.19
	112	12.16	46.9665	21.188	14.4412	27.743	0.14
	113	12.16	46.6537	20.600	14.1287	27.132	0.15
	114	12.24	47.4024	21.939	14.8769	28.525	0.39
	115	12.51	47.2698	17.198	14.7458	23.775	0.13
	116	12.72	47.0583	22.027	14.5328	28.589	0.19
	117	12.86	47.0778	21.726	14.5523	28.288	0.14
	118	13.07	46.8463	20.094	14.3215	26.640	0.17
	119	13.56	47.4364	18.336	14.9120	24.924	0.17
	120	13.56	46.7487	19.915	14.2239	26.454	0.22
	121	13.56	47.0897	21.697	14.5643	28.260	0.13
	122	13.99	47.0696	22.149	14.5440	28.711	0.36
	123	14.27	46.8284	10.361	14.3066	16.906	0.10
	124	14.39	47.0897	22.426	14.5641	28.989	0.35
	125	14.76	46.7700	19.827	14.2452	26.367	0.28
	126	15.67	47.0976	22.393	14.5720	28.957	0.15
	127	15.67	46.8512	19.455	14.3265	26.001	0.12
	128	15.67	46.7914	19.479	14.2667	26.021	0.12
	129	15.67	47.1407	22.790	14.6149	29.357	0.09
	130	15.67	47.1195	22.518	14.5938	29.083	0.10
	131	15.83	47.3816	21.585	14.8562	28.169	0.49
	132	16.38	47.1348	22.297	14.6092	28.864	0.16
	133	16.38	47.0745	21.293	14.5492	27.855	0.11
	134	16.73	47.1427	21.852	14.6172	28.419	0.14
	135	16.73	47.4460	21.058	14.9208	27.647	0.10
	136	16.73	47.1279	22.473	14.6022	29.039	0.14
	137	17.08	47.1074	22.284	14.5818	28.849	0.12
	138	17.30	47.1830	21.759	14.6576	28.329	0.49
	139	17.43	46.7458	19.202	14.2212	25.740	0.10
	140	17.43	47.2621	22.741	14.7363	29.317	0.11
	141	17.52	47.2124	22.805	14.6866	29.377	0.33
	142	17.70	47.1094	22.098	14.5839	28.662	1.33
	143	17.76	47.2777	23.112	14.7518	29.689	0.16
	144	17.85	47.1364	22.364	14.6108	28.931	1.05
	145	17.89	47.0646	22.633	14.5389	29.194	0.26
	146	17.99	46.6726	20.281	14.1477	26.814	0.18
	147	18.49	47.1717	22.117	14.6462	28.687	0.11
	148	18.49	47.1378	24.08s	14.6116	30.649	0.11
	149	18.49	46.9396	11.550	14.4174	18.103	0.10

Table 1. OH 1.6-GHz Masers in Orion-BN/KL, continued.

Transition	Feature No.	Velocity (km s^{-1})	RA(1950) 05^h32^m ^{s}	Dec(1950) –5°:24′: ″	RA(2000) 05^hh35^m ^{s}	Dec(2000) –5°:22′: ″	Intensity (Jy $beam^{-1}$)
1665R	150	18.49	47.2269	22.836	14.7011	29.409	0.12
	151	18.49	47.1035	23.022	14.5776	29.586	0.10
	152	18.49	47.1097	23.543	14.5836	30.108	0.08
	153	18.49	47.3616	21.744	14.8361	28.327	0.12
	154	18.49	47.0872	24.091	14.5610	30.655	0.08
	155	18.63	47.1870	23.139	14.6611	29.709	0.23
	156	18.64	47.1385	22.269	14.6128	28.836	7.34
	157	18.76	47.1659	22.942	14.6401	29.511	0.77
	158	18.84	47.1304	21.627	14.6050	28.194	0.10
	159	18.84	46.6699	20.266	14.1449	26.799	0.12
	160	18.84	47.1244	23.040	14.5986	29.606	0.15
	161	18.84	47.1112	22.301	14.5856	28.867	0.12
	162	18.84	47.1303	23.436	14.6043	30.002	0.09
	163	18.84	47.0534	23.996	14.5273	30.557	0.10
	164	19.03	46.7193	19.180	14.1947	25.716	0.18
	165	19.19	47.3167	22.621	14.7910	29.201	0.11
	166	19.19	47.0641	22.715	14.5383	29.276	0.09
	167	19.35	46.9618	21.237	14.4365	27.792	0.11
	168	19.42	47.3386	22.245	14.8129	28.826	0.21
	169	19.46	47.1366	22.211	14.6110	28.778	0.37
	170	19.54	47.1549	22.679	14.6292	29.247	0.16
	171	19.54	47.2993	23.040	14.7734	29.618	0.10
	172	19.54	47.2746	22.420	14.7489	28.997	0.25
	173	19.54	46.6645	19.663	14.1398	26.196	0.11
	174	19.54	47.0678	22.465	14.5422	29.027	0.16
	175	19.54	47.3164	22.148	14.7909	28.728	0.09
	176	19.54	47.1038	22.720	14.5780	29.284	0.16
	177	19.71	47.1870	23.004	14.6612	29.575	0.39
	178	19.89	47.2796	21.609	14.7542	28.187	0.10
	179	19.89	47.3264	22.292	14.8008	28.872	0.11
	180	20.00	47.2892	22.323	14.7635	28.901	4.24
	181	20.06	47.2165	23.524	14.6905	30.097	0.18
	182	20.09	46.9299	14.804	14.4068	21.356	0.12
	183	20.24	47.1416	22.404	14.6159	28.972	0.21
	184	20.24	47.3210	22.020	14.7954	28.600	0.38
	185	20.24	47.3613	21.756	14.8359	28.339	0.10
	186	20.24	46.8675	20.300	14.3425	26.848	0.11
	187	20.24	47.2083	22.882	14.6825	29.454	0.20
	188	20.24	47.2757	22.359	14.7500	28.936	0.23
	189	20.24	47.2389	23.568	14.7129	30.142	0.14
	190	20.49	46.8274	19.833	14.3026	26.378	0.34
	191	20.60	47.2254	22.594	14.6997	29.167	0.28
	192	20.61	47.1927	22.700	14.6670	29.271	0.28
	193	20.73	47.0252	18.005	14.5010	24.563	0.17
	194	20.78	47.2590	22.030	14.7335	28.605	0.59
	195	20.79	47.1323	22.381	14.6066	28.947	0.32
	196	20.95	47.1747	22.706	14.6489	29.276	0.12
	197	21.11	47.3075	21.887	14.7820	28.466	0.72
	198	21.30	47.2234	23.040	14.6976	29.613	0.10
	199	21.30	47.2034	23.131	14.6775	29.703	0.10
	200	21.30	47.1751	22.577	14.6494	29.147	0.31

Table 1. OH 1.6-GHz Masers in Orion-BN/KL, continued.

Transition	Feature No.	Velocity (km s^{-1})	RA(1950) 05^h32^m ^{s}	Dec(1950) $-5°$:24′: ″	RA(2000) 05^hh35^m ^{s}	Dec(2000) $-5°$:22′: ″	Intensity (Jy $beam^{-1}$)
1665R	201	21.38	47.2850	21.772	14.7596	28.350	1.48
	202	21.51	46.7892	19.337	14.2645	25.879	0.18
	203	21.65	46.7448	18.535	14.2205	25.074	0.14
	204	22.00	47.1648	22.167	14.6392	28.736	0.15
	205	22.00	47.2413	21.959	14.7158	28.534	0.15
	206	22.00	47.1936	22.864	14.6678	29.435	0.12
	207	22.00	47.1771	21.131	14.6518	27.701	0.22
	208	22.01	46.7630	18.902	14.2385	25.442	0.19
	209	22.22	47.3115	21.333	14.7862	27.913	0.29
	210	22.35	46.7742	19.028	14.2497	25.569	0.11
	211	22.35	46.8020	19.538	14.2773	26.081	0.08
	212	22.50	47.1623	21.593	14.6369	28.162	2.19
	213	22.54	46.6625	23.668	14.1364	30.201	0.84
	214	22.58	47.2731	21.427	14.7478	28.004	0.20
	215	22.70	47.2730	20.298	14.7480	26.875	0.09
	216	22.70	46.7332	18.448	14.2089	24.986	0.11
	217	22.70	46.7309	20.211	14.2060	26.748	0.10
	218	22.70	46.8040	19.311	14.2794	25.854	0.09
	219	22.70	47.2795	19.234	14.7549	25.811	0.31
	220	22.81	47.3016	21.029	14.7764	27.608	0.25
	221	22.86	47.3174	21.643	14.7920	28.223	0.26
	222	23.06	46.8216	19.733	14.2968	26.277	0.13
	223	23.06	47.0926	21.834	14.5671	28.397	0.09
	224	23.06	46.8102	19.504	14.2855	26.047	0.10
	225	23.57	47.3143	19.297	14.7897	25.877	0.10
	226	23.65	47.3609	19.201	14.8363	25.784	0.31
1667L	1	13.46	46.9359	24.607	14.4096	31.159	0.30
	2	13.51	46.9845	24.415	14.4582	30.971	0.21
	3	13.43	46.9832	29.620	14.4552	36.176	.21